

AN ABSTRACT OF THE THESIS OF

J Kenneth Trolan for the Ph.D in Physics  
(Name) (Degree) (Major)

Date Thesis Presented May 12, 1950

Title EXTENSION OF THE EXPERIMENTAL FIELD-CURRENT LAW TO REGIONS  
OF HIGH FIELDS AND LARGE CURRENTS

Abstract Approved [REDACTED]  
(Major Professor)

Experiments are described for investigating the validity of the theoretical field emission law at high electric fields and large currents. Tungsten point to plane field emitters have been used over the current ranges from 0.5 to 88 and from  $10^{-8}$  to  $10^{-3}$  milliamperes thus extending considerably the range of previous experimental observations. Pulse techniques were used for the higher current range. The size of the emitting areas are calculated to be of the order of  $10^{-9}$  to  $10^{-12}$   $\text{cm}^2$  while current densities are found to be as high as  $6 \times 10^9$  amperes per  $\text{cm}^2$ . These values are in substantial agreement with those previously reported under similar conditions. The theoretical law governing field emission is found to agree in order of magnitude with experiment. When the upper field limit is approached, the potential barrier is reduced to the level of the most energetic free electrons within the metal and a vacuum arc ensues which in most cases vaporizes the emitter point. In one case, during an arc, an emitter withstood without apparent change in characteristics, an instantaneous current estimated at 100 amperes. Heating effects at the emitter surface caused by large emission current densities are noted. Electron microscope types of field emission tubes have been used to compare visually the emission pattern for emitters under direct current conditions with those obtained under pulsed conditions.

EXTENSION OF THE EXPERIMENTAL FIELD-CURRENT LAW  
TO REGIONS OF HIGH FIELDS AND LARGE CURRENTS

by

J KENNETH TROLAN

TJUV

A THESIS

submitted to

OREGON STATE COLLEGE

in partial fulfillment of  
the requirements for the  
degree of

DOCTOR OF PHILOSOPHY

June 1950

APPROVED:

  
\_\_\_\_\_  
Professor of Physics

In Charge of Major

  
\_\_\_\_\_  
Head of Department of Physics

  
\_\_\_\_\_  
Chairman of School Graduate Committee

  
\_\_\_\_\_  
Dean of Graduate School

Typist \_\_\_\_\_

#### ACKNOWLEDGMENT

The author wishes to express his gratitude to Dr. E. A. Yunker for his time, thought and guidance on the project, and to Dr. W. P. Dyke for suggesting the research problem and for his able supervision of the work.

The use of the research facilities of Linfield College and the support of this work by the Office of Naval Research are both appreciated.

## TABLE OF CONTENTS

	Page
INTRODUCTION. . . . .	1
A PULSE METHOD FOR INVESTIGATING FIELD EMISSION . . . . .	15
The Time-Marker Circuit. . . . .	17
The Trigger Amplifier and Pulse Generator. . . . .	20
Voltage Dividers . . . . .	22
Current Pick-up Devices. . . . .	25
Photographic Recording . . . . .	29
Experimental Tubes . . . . .	30
Calibrations . . . . .	40
EXPERIMENTAL PROCEDURE. . . . .	43
EXPERIMENTAL RESULTS. . . . .	45
Table 1. . . . .	52
Table 2. . . . .	59
SUMMARY . . . . .	81
BIBLIOGRAPHY. . . . .	84

## LIST OF FIGURES

<u>Figure</u>	<u>Page</u>
1. Force and potential energy for an electron in the vicinity of an isolated nucleus. . . . .	4
2. Potential energy of an electron along a line through two adjacent atoms . . . . .	4
3. Potential energy of an electron along a line through a row of atoms in a metal. . . . .	4
4. Electron energy distribution in tungsten at 0° and 2500° K. . . . .	6
5. Energy level diagram of the free electrons within a metal. . . . .	6
6. The potential energy curves with and without an applied electric field at the surface of a cold metal. . . .	7
7. Block diagram of trigger and time-marker generator . . . .	7
8. Combined block and schematic diagram of pulse generator. .	18
9. Schematic diagram of trigger and time-marker generator . .	19
10. Schematic diagram of trigger amplifier and pulse generator. . . . .	21
11. Pulse generator. . . . .	23
12. Various types of voltage divider . . . . .	24
13. Type IN34 crystal curves . . . . .	27
14. Type IN21A crystal curves. . . . .	27
15. Direct current and pulse calibrations of IN34 type crystals . . . . .	28
16. Point to plane field current tube. . . . .	31
17. Point to plane field current tube. . . . .	32
18. Five point field current tube. . . . .	32
19. Five point field current tube. . . . .	33

<u>Figure</u>	<u>Page</u>
20. Electron microscope type tube. . . . .	35
21. Electron microscope type tube. . . . .	36
22. Linear filament type tube. . . . .	36
23. Linear filament type tube. . . . .	37
24. Arrangement of equipment for data run. . . . .	38
25. Typical current and voltage pulses from oscilloscope photographs. . . . .	46
26. Relationship between $\log_e i$ and reciprocal voltage for a direct current tungsten field emitter. . . . .	47
27. Relationship between $\log_e i$ and reciprocal voltage showing reproducibility of data for several pulses from a single emitter. . . . .	47
28. Relationship between $\log_e i$ and reciprocal voltage for field emitter #1, for both pulsed and d-c operation. . . . .	48
29. Relationship between $\log_e i$ and reciprocal voltage for field emitter #2, for both pulsed and d-c operation. . . . .	49
30. Relationship between $\log_e i$ and reciprocal voltage for field emitter #3, for both pulsed and d-c operation. . . . .	50
31. Graph of $\log_e i$ versus reciprocal voltage showing comparison of experimental curves with theoretical curves . . . . .	53
32. Electron microscope projection of emitting cathode surface showing emission from small spots of im- purities of low work function. From Müller (16, p. 545) . . . . .	62
33. Typical examples of blunt remains of previously sharp tungsten points after passage of vacuum arc. Magnification 680x. . . . .	68
34. Normal behavior below region of instability. . . . .	69
35. Behavior during vacuum arc which emitter survived. . . . .	69
36. Normal behavior below region of instability after surviving arc. . . . .	69

<u>Figure</u>	<u>Page</u>
37. Behavior during second arc which destroyed emitter. . . . .	69
38. Voltage and current oscilloscope traces during four vacuum arcs of three different emitters . . . . .	72
39. Normal pulse condition below region of instability. . . . .	74
40. Abnormal pulse condition bordering region of instability. . . . .	74
41. Pulse condition during vacuum arc . . . . .	74
42. Emitter point before use in electron microscope tube. Magnification 2000x.. . . . .	78
43. Emitter point after use in electron microscope tube. Magnification 1500x.. . . . .	78
44. Emission patterns from electron microscope type field emission tube for different linear tungsten wire emitters . . . . .	80
45. Electron microscope photomicrograph of typical, sharp, tungsten point field emitter. . . . .	83

EXTENSION OF THE EXPERIMENTAL FIELD-CURRENT LAW  
TO REGIONS OF HIGH FIELDS AND LARGE CURRENTS

INTRODUCTION

Electron emission from metals may be classified into four types: 1. Thermal emission, 2. Photoelectric emission, 3. Secondary emission, 4. Field emission.

The laws governing the first two types are fairly well established. However the latter two are not so well understood. This thesis deals specifically with the fourth type.

Field emission occurs where the electric field at the surface of the metal is in such a direction as to accelerate electrons away from the metal, its magnitude, computed geometrically, being about a million volts per centimeter.

In order to appreciate the theoretical laws governing field emission, it is necessary to consider briefly the existing knowledge concerning the structure of metals. Metals are considered to be crystalline structures consisting of orderly three dimensional spacial arrays of atoms or ions. These ions are located so close together that their valence electrons are either completely disassociated from the atoms, or at best only very loosely bound to them. Thus the valence electrons are free within the metal and move about between the ions which are fixed.

Each atom may yield one, two, or sometimes three valence electrons, which thus become the free electrons of the metal. Usually about  $10^{22}$  electrons per  $\text{cm}^3$  are free to move. These so

called conduction electrons constitute what is frequently referred to as an electron gas; their motion may constitute an electric current.

Because of the existence of ions within the metal, the early concept that the interior of a metal has a uniform potential must be discarded in favor of a more complicated distribution.

The attractive force between a nucleus of atomic number  $Z$ , and an electron, is given by Coulomb's law:

$$f = \frac{ZQ_e Q_e}{\epsilon_0 r^2}$$

where  $f$  is the attractive force,

$Q_e$  the electronic charge,

$r$  the distance between the nucleus and the electron, and

$\epsilon_0$  the permittivity of free space. (5, p. 64-75).

The potential energy of the electron is expressed by the equation

$$w = \frac{ZQ_e^2}{\epsilon_0 r}$$

where the potential energy of the electron is assumed to be zero at infinity. Thus for a single atom, the potential energy and fields of force would appear as in Fig. 1. A curve of  $W$  as a function of  $r$  is shown for two closely spaced atoms in Fig. 2. Figures 1, 2, and 3 are from (5, p. 65-65).

A two dimensional picture of the potential energy distribution inside and at the surface of a metal consisting of many closely

spaced ions can be constructed as in Fig. 3 (15, p. 118), (5, p. 65). The potential energy curve consists of a series of humps similar to the single hump of Fig. 2. Because of the absence of further nuclei beyond the surface of the metal, the potential energy approaches zero for increasing values of  $r$ . An electron with energy corresponding to that of point A at the level a-b of Fig. 3, is free to move back and forth but encounters potential energy barriers at (a) and (b) and thus cannot escape. Such an electron is tightly bound to the nucleus and cannot contribute to the conductivity of the metal. A free, or conduction electron, corresponding to the point B of Fig. 3 is free to move about within the confines of the metal, but upon nearing a boundary of the metal will encounter a potential energy barrier which it cannot surmount unless it receives additional energy. This barrier is known as the surface barrier. Since the bound electrons have very little chance to escape from the metal, consideration will be given to the so-called "free" electrons.

Fermi (7, p. 902-912) and Dirac (3, p. 661-677) in independent investigations deduced an energy density function which adequately describes the state of the free electrons in the metal at all times. Figure 4 is a plot of this distribution function for tungsten at  $0^{\circ}\text{K}$ . The number of electrons per unit volume of metal having any particular energy  $W$  is represented by  $\rho_e$  and the maximum energy that any electron in the metal can have at  $0^{\circ}\text{K}$ , by  $\mu$ . It is observed that even at absolute zero, electrons may have energies ranging from zero up to  $\mu$ , the greatest number of electrons having energies near  $\mu$ .

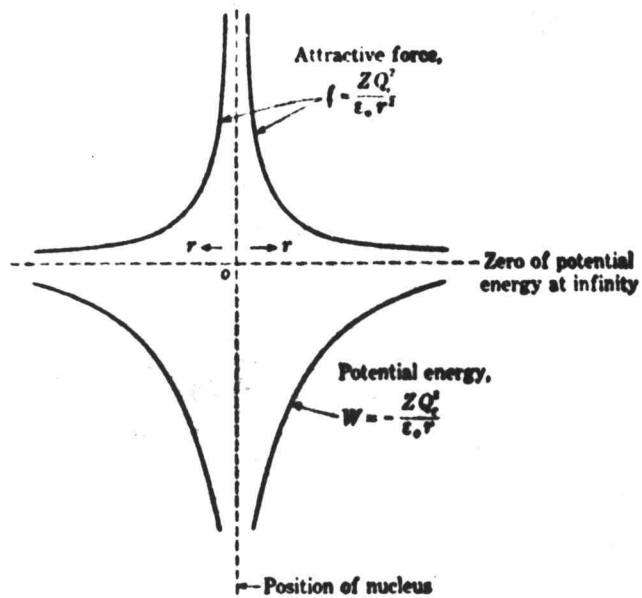


Fig. 1 Force and potential energy for an electron in the vicinity of an isolated nucleus.

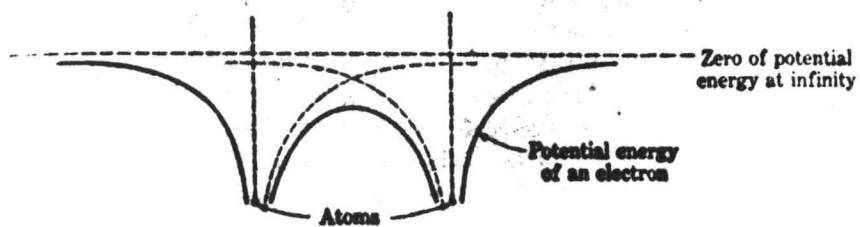


Fig. 2 Potential energy of an electron along a line through two adjacent atoms.

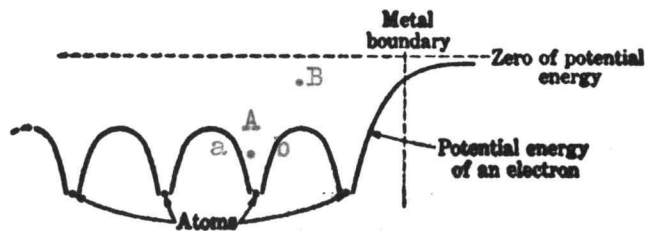


Fig. 3 Potential energy of an electron along a line through a row of atoms in a metal.

In order to escape from the surface of the metal, an electron may, as in the case of thermal, photoelectric, or secondary emission, acquire in some manner sufficient energy to surmount the potential energy barrier, or it may penetrate a "thinned barrier" as in field emission. The minimum amount of energy that must be imparted to an electron at absolute zero in order to permit it to surmount the barrier and escape from the metal, is known as the work function of the metal, and is designated by  $\phi$  in Fig. 5.

The barriers, as represented in Figs. 3 and 5, are infinitely thick. However, it is possible to make the barrier finite in thickness and in some cases relatively thin, and to simultaneously reduce the barrier height, by creating an accelerating electric field at the surface of the metal.

Figure 6 compares the surface barrier of the metal for a condition of no external field with that for an accelerating electric field.

When an electron in a metal impinges on a surface potential barrier with a velocity normal to the surface, wave mechanics predicts that a probability exists that the electron will emerge from the metal without change of energy. This process is called "tunneling" and its probability of occurrence depends upon the energy of the electron associated with its motion normal to the barrier, and upon the barrier's height, thickness and general shape. It is possible to obtain a barrier transmission coefficient and, by summing over the various electron energies, to obtain a theoretical relationship for emitted current density,  $J$ , in terms of applied electric

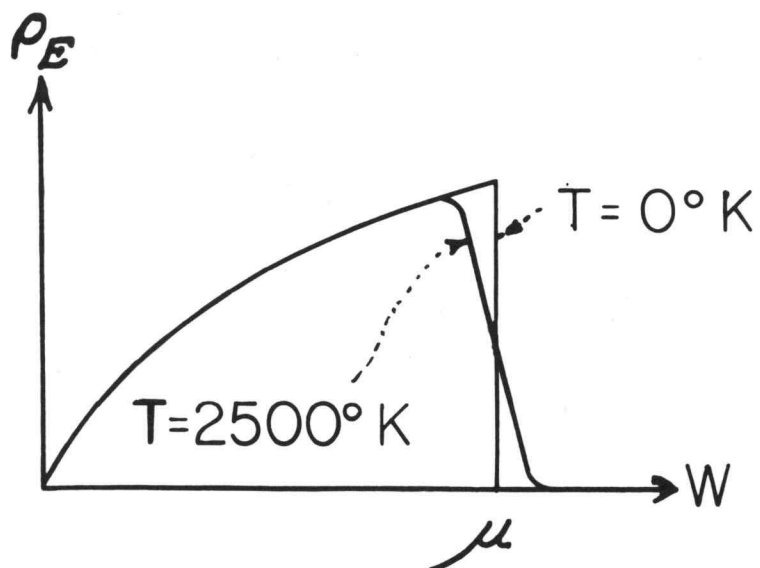


Fig. 4 Electron energy distribution in tungsten at  $0^\circ$  and  $2500^\circ \text{K}$ .

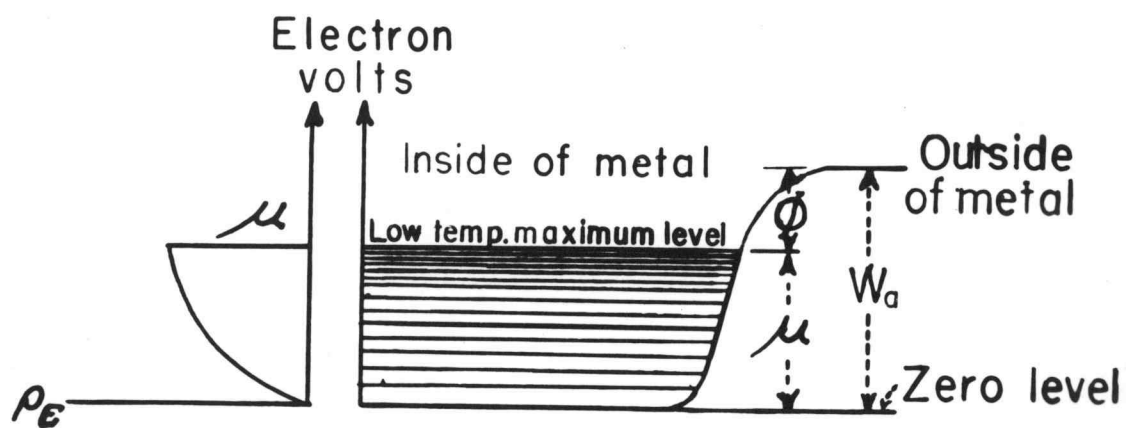


Fig. 5 Energy level diagram of the free electrons within a metal.



field  $F$  and other parameters. Fowler and Nordheim (9, p. 173-181) and Nordheim (17, p. 626-639), following this procedure, obtained the expression

$$J = 6.2 \times 10^{-6} \frac{\mu_0^{1/2}}{(\phi + \mu) \phi^{1/2}} F^2 e^{-\frac{6.8 \times 10^7 \phi^{3/2}}{F}} f(y)$$

where

$J$  = current density in amperes/cm<sup>2</sup>.

$F$  = electric field in volts/cm.

$\phi$  = work function in electron volts.

$$f(y) = \sqrt{\frac{1+\sqrt{1-y^2}}{2}} \left[ E(k) - \frac{y^2}{1+\sqrt{1-y^2}} K(k) \right]$$

$$y = \sqrt{\frac{e F}{\phi}}; \quad k = \frac{2\sqrt{1-y^2}}{1+\sqrt{1-y^2}} \quad \text{and}$$

$$K(k) = \int_0^{\pi/2} (1-k^2 \sin^2 \theta)^{-1/2} d\theta$$

$$E(k) = \int_0^{\pi/2} (1-k^2 \sin^2 \theta) d\theta$$

Numerous experiments have been performed to check the theory of Fowler and Nordheim. The early work of Millikan and Lauritsen (11, p. 45-49), Millikan and Eyring (8, p. 52-67), Eyring, MacKeowan and Millikan (9, p. 900-909) and the Staff of the General Electric Company of London (10, p. 609-635) left little doubt that, at relatively low current densities, the total field current is related to the geometrically computed applied field by the empirical equation

$$I = Ce^{-b/F}$$

where  $C$  and  $b$  are constants. The theoretical equation of Fowler and Nordheim reduces to this form at low current densities since in this region  $f(y)$  is nearly unity and the effect of the  $F^2$  term is negligible compared to that of the exponential term.

That the electrons in field emission are emitted without change in energy has been established experimentally by Henderson and Fleming (16, p. 887-894). This concept is basic to the wave mechanical theory of field emission.

The distribution in energy among the emitted field electrons has been measured by Henderson and Dahlstrom (12, p. 473-481) and by Dyke (4, p. 39-44) and found to be in good agreement with the energy distribution predicted by Fowler and Nordheim. This agreement is further regarded as an experimental confirmation of the distribution in energy among the free electrons in metals, as predicted by Fermi (7, p. 902-912) and Dirac (3, p. 661-677).

Stern, Gossling and Fowler (20, p. 699-723) have made a detailed experimental study of the theoretical field emission equation. By varying the work function of the emitter they found good agreement in the dependence of the total emission current upon work function. They were able, by combining the results of several experimenters with theory, to arrive at values for the current density  $J$  and area  $A$  for the various emitters used. They have reported areas between  $8 \times 10^{-8}$  and  $1.2 \times 10^{-10}$   $\text{cm}^2$  and current densities between  $1 \times 10^2$  and  $2.1 \times 10^7$   $\text{amps/cm}^2$  and have concluded that the effects of space charge are negligible except, perhaps, in one or two cases where unusually

large current densities were observed.

When the emitting surfaces are pure, the field emission is found to be independent of temperature up to temperatures approaching thermal emission values (13, p. 59-60), (2, p. 239-240). However when the emitting surfaces are contaminated, a so-called "fugitive temperature" effect exists. This has been reported by Stern, Gossling and Fowler (20, p. 722-723) and Dyke (4, p. 54-55). Under these conditions a change in temperature from 300°C to 700°C may change the current reversibly by as much as a factor of 100.

The emitting area, current density and emission pattern from a point emitter were examined in detail by Müller, using a tube similar in principle to an electron microscope, which projected the emission pattern upon a fluorescent screen with a magnification of  $2 \times 10^5$ .

Emissions from various crystal faces were found to depend upon the work functions of each face and were enhanced by spots of impurities, or decreased by adsorbed oxygen. By direct observation, the emitting areas of the various small spots were found to be as low as  $10^{-11}$  cm<sup>2</sup> with corresponding current densities as high as  $10^6$  amperes/cm<sup>2</sup>.

Müller concludes that when the tungsten point is sharpened by electrolytic etching, the whole point area emits, and that there are no rough projections on its surface.

The foregoing experiments, in which continuous voltages were used, show in nearly every case reasonably good comparison with theory. With one exception these empirical observations were made at relatively low current densities.

The behavior of the field emitter at very high current densities and electric fields is of unusual interest in view of the theory of Fowler and Nordheim. At electric fields approaching  $10^8$  volts/cm the effect of the  $F^2$  term in the theoretical equation becomes significant. Thus at these high electric fields one might expect a departure from linearity of  $\log_e J$  as a function of  $\frac{1}{F}$ . This departure is in the direction of more current for a given voltage. However, Stern, Gossling and Fowler have shown from theoretical considerations, that the space charge due to large emitted current densities may be great enough to appreciably reduce the electric field near the emitter. This is true for fields approaching  $10^8$  volts/cm and results in the emission of less current at any given voltage than would otherwise be expected.

The behavior of the emitter when the electric field reaches the value  $F = 7 \times 10^6 \phi^2$  is of special interest. Thus for tungsten for which the work function is 4.5 volts, the field value from the above expression would be  $1.42 \times 10^8$  volts, at which, according to the theory of Fowler and Nordheim, the surface barrier is reduced to a level corresponding to that of the top electron energy for zero temperatures. Thus it would appear that at fields above this critical value, the most energetic electrons in the metal have energies greater than that of the surface barrier. The transmission coefficient for these electrons is thus greatly increased. In fact, at fields greater than  $7.0 \times 10^6 \phi^2$ , the theory of Fowler and Nordheim no longer applies, and predictions of the behavior of the field emitter must be sought elsewhere.

The transmission coefficient for an electron whose energy is greater than that of the surface barrier is shown by Rojansky (19, p. 218) to rapidly approach unity as the electron energy reaches a value of roughly ten times the barrier value. This is of course a much larger coefficient than in the case in which the electron energy is less than that of the barrier. Thus one might expect the emitted field current to increase markedly as the electric field approaches  $F = 7.0 \times 10^6 \phi^2$ . In view of the large number of free electrons in a metal (roughly  $10^{22}$  per c.c.) the available current might be expected to be phenomenally large under these conditions.

Several experiments have been performed (1, p. 113-118) (20, p. 699-723) in the attempt to test the theory of Fowler and Nordheim at large current densities and high electric fields, and worthwhile progress has been made. It is generally difficult, however, to extract currents of very large densities, using direct current methods, because of the instability of the field emitter. In spite of the inability to reach very large current densities some comparison of the dependence of the current density upon the exponential term and the term in  $F^2$  in the theory has been made by examining the behavior of the emitter over a very large current range.

Millikan and Eyring (13, p. 55) examined the behavior of the field emitter over the range of currents extending from  $10^{-11}$  to  $6 \times 10^{-4}$  amperes. Upon re-examination of these data, Stern, Gossling and Fowler (20, p. 700) conclude that they fit the relationship

$$I = AF^2 e^{-b/F}$$

where

$I$  is the total current in amperes,

$F$  the electric field in volts/cm,

$A$ , and  $b$  are constants.

This is in agreement with the theory of Fowler and Nordheim. The maximum current density obtained by Millikan and Eyring is computed to be  $9 \times 10^6$  amperes/cm<sup>2</sup>.

Abbott and Henderson (1, p. 117) extended the range of observed field currents from  $10^{-17}$  to  $10^{-5}$  ampere and conclude that the functional dependence of the total field current emission upon the field is best represented by an equation of the form

$$I = CF^A e^{-b/F}$$

where the symbols have the meanings already given. They note that their observations are not necessarily in disagreement with the theory of Fowler and Nordheim since this theory describes current density  $J$  whereas Abbott and Henderson dealt with total current from a relatively large emitting area or areas. The maximum current density is  $8 \times 10^3$  amperes/cm<sup>2</sup>, which is relatively low.

There is one isolated reference in the literature to direct current field emission in which total currents extending from  $10^{-3}$  to  $4 \times 10^{-2}$  amperes, with a maximum current density as high as  $2 \times 10^7$  amperes/cm<sup>2</sup> are reported. This performance is remarkable indeed in view of the more usual behavior of the direct-current field emitter. The area of the emitter was calculated to be  $1.2 \times 10^{-10}$  which is in reasonable agreement with those observed by Müller.

It is the purpose of this thesis to observe the behavior of field emitters at the highest possible values of electric field and resulting current density. A comparison between experimental results and theoretical predictions is made in order to test the existing theory and extend it where necessary.

At the higher densities currents are drawn for only a few millionths of a second. This technique limits the undesirable effects of emitter heating and deterioration caused by positive ion bombardment and by conduction currents through the emitter. It is thus possible to subject the emitters to electric fields of sufficient magnitude to reduce the metallic surface barrier by an amount approaching  $\phi$  so that unusually large field currents may be obtained. The effects of space charge and emitter heating are considered. An electron microscope type of tube is used to study the emission patterns of pulsed emitters.

## A PULSE METHOD FOR INVESTIGATING FIELD EMISSION

In order to test the theoretical field current law it is necessary to find values of total current for corresponding values of voltage. If pulse methods are employed, the instantaneous magnitudes of these quantities must be determined during the pulse time. The cathode ray oscillograph suggests itself for this purpose, and has been successfully employed in these experiments.

A voltage pulse having a saw-tooth shape is desirable in order to obtain data at several different voltages during a single pulse. A method of obtaining satisfactory pulse shape is to discharge a capacitor through a fixed resistance. The voltage developed across the resistance decays exponentially from the capacitor's initial voltage to about 30% of the initial voltage in  $RC$  seconds, where  $R$  is the resistance in ohms and  $C$  the capacitance in farads. Thus the value of either  $R$  or  $C$ , or both, may be adjusted to produce the desired pulse length.

The voltage pulse is reduced by means of a capacitance divider and recorded on an oscillograph.

The corresponding pulse of current is passed through a "current pick-up impedance" and the voltage produced across this impedance is applied directly to the vertical deflection plates, or amplifiers, of another oscilloscope tube.

The horizontal axis of each oscilloscope tube represents time. Thus one oscilloscope presents voltage as a function of time and the other current as a function of time. Since the relationship between

current and voltage is desired, it is necessary to remove the time parameter by determining the value of current for a given voltage. This was done by generating time markers which blank the two oscilloscope traces, simultaneously and periodically, for short intervals during each trace. These time markers caused the traces to appear as broken lines as in Fig. 25. The oscilloscope traces are photographed by two 35 mm, f 2.3. Fairchild Type A Oscilloscope Recording Cameras equipped with automatic shutters and film advance mechanisms. The values of current and voltage at corresponding pairs of time markers were determined from the photographs.

The data were gathered on a "one-shot" basis. The timing sequence was arranged such that closing a telegraph key opened the camera shutter, started the two oscilloscope sweeps and the time-marker generator, triggered the high voltage pulse generator, applied the pulse to the field current tube, closed the shutter, and advanced the film.

A combined block and schematic diagram of the pulser and its associated circuits is shown in Fig. 8. The d-c voltage generator was used to charge the 0.25 mf capacitor, through the 2 megohm resistor, to any desired voltage between zero and sixteen thousand volts. The 5C22 hydrogen thyratron tube acts as a switch that can be closed so as to discharge the capacitor through the 50 ohm shunting resistor thus applying the condenser voltage to the field current tube. Figure 24 is a photograph of the apparatus.

### The Time-Marker Circuit

Figure 7 is a block diagram and Fig. 9 is the schematic diagram of the trigger generator and time-marker generator. A one-shot multivibrator is triggered by means of a telegraph key. The multivibrator executes one complete cycle and returns to its initial quiescent state. The output wave from the multivibrator turns on two oscillators, one having a frequency of 1.0 megacycles/sec, the other 0.1 megacycles/sec. The outputs from the two oscillators are separately clipped, squared, differentiated after which they are further clipped so that one sharp positive spike is produced for each cycle of each oscillator. The 1.0 megacycle oscillator produces voltage spikes at 1 micro-second intervals while the 0.1 megacycle oscillator produces them at 10 micro-second intervals. These voltage spikes are applied to the cathodes of the cathode-ray-tubes thus providing intensity modulation of the trace in the form of blank spots at one and ten micro-second intervals as shown in Fig. 25.

The trailing edge of the multivibrator output pulse also generates a trigger voltage which starts the oscilloscope sweeps and triggers the 5C22 thyratron.

In order to produce sharp one micro-second marker pulses stray capacitance and inductance effects must be minimized. The frequency content of such a train of voltage spikes should include the 1.0 megacycle/sec fundamental as well as its harmonics up to at least the 15th. All the circuits utilized as square and clip this wave to produce the micro-second voltage spikes must necessarily pass this band

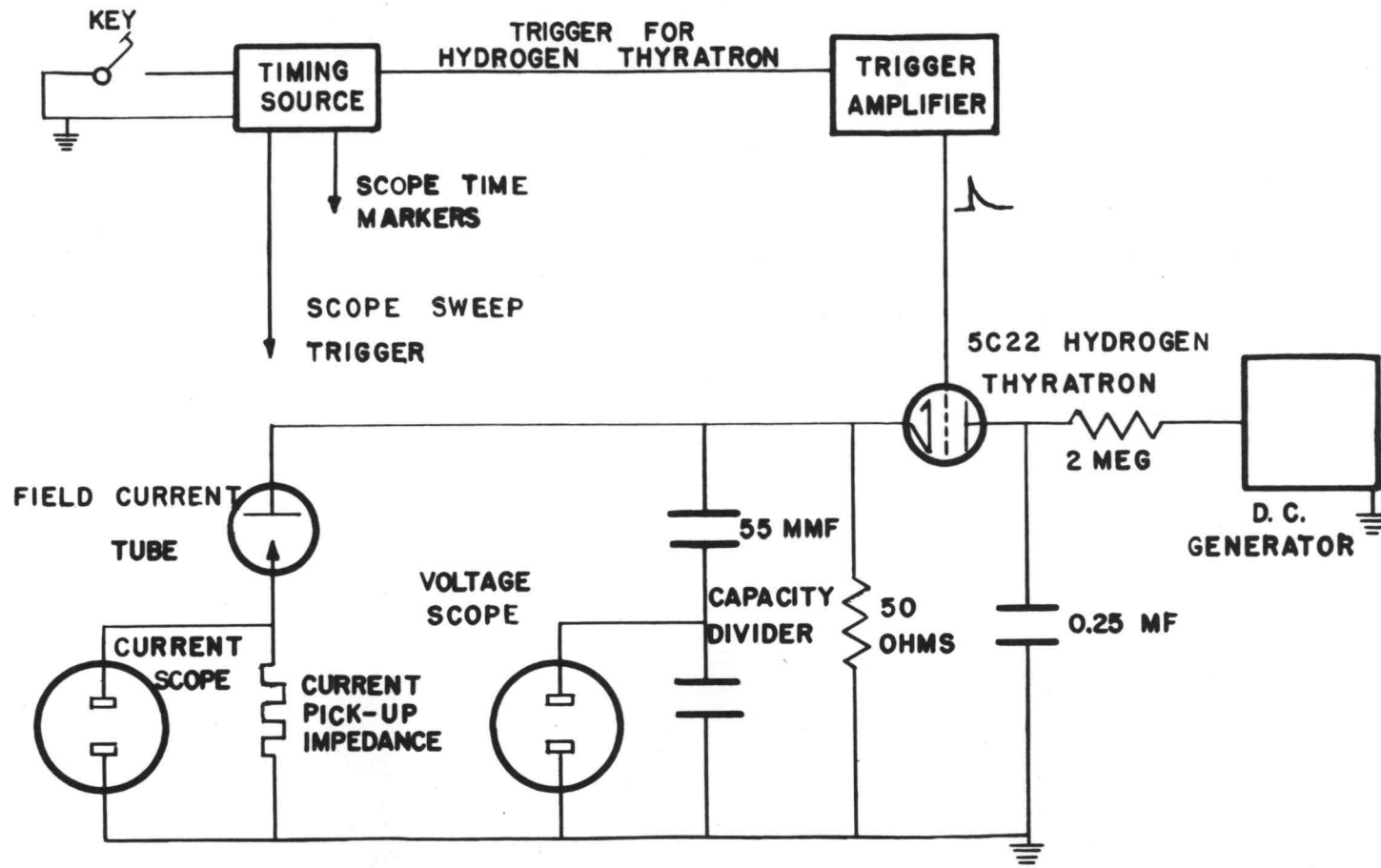


Fig. 8 Combined block and schematic diagram of pulse generator.

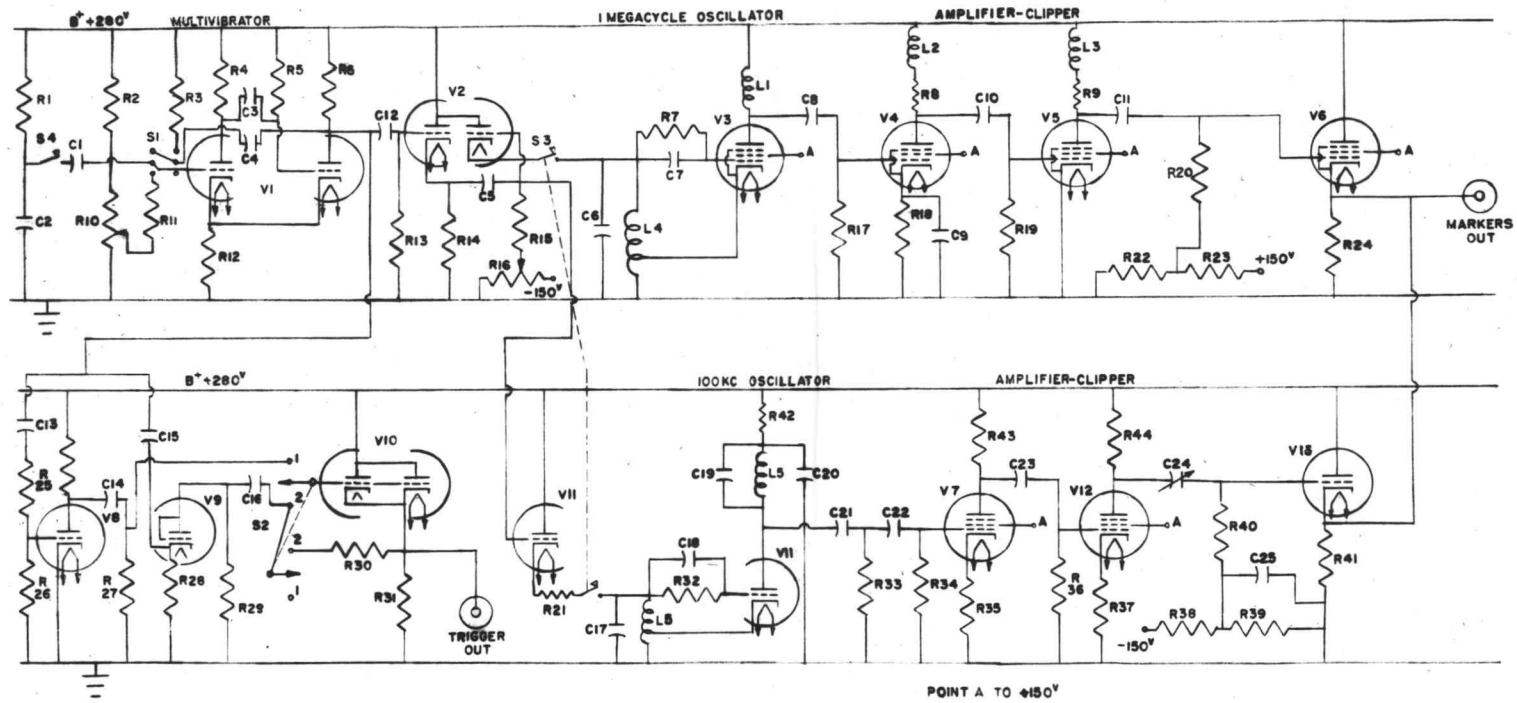


Fig. 9 Schematic diagram of trigger and time-marker generator.

of frequencies. This requires high frequency compensation, low plate loads, low gain per stage of amplification as well as care in keeping shunt capacities and lead inductances as low as possible.

#### The Trigger Amplifier and Pulse Generator

The trigger amplifier and pulse generator are represented schematically in Fig. 10. These circuits are treated in considerable detail since they introduce rather difficult clipping problems. The trigger pulse which is generated by the timing circuit is amplified by the 6L6 amplifier of Fig. 10. The amplified trigger voltage is applied to the grid of the 5022 causing this tube to conduct. During the conduction period the potentials of the cathode and grid of the tube rise to the peak pulse voltage which may be as high as 15,000 volts. This rapid voltage rise of the grid and cathode generates a pulse which travels in a reverse direction through the trigger amplifier. In order to prevent arc-over in the trigger amplifier every time the system is fired it was necessary to introduce the 715 B diode clipper tubes of Fig. 10. One 715B prevents the back voltage from rising above B + potential (560 volts), the other prevents the back voltage from going below ground potential. Type 715 B tubes, which are capable of supplying peak currents of 10 amperes, were used in order to prevent the charging of the stray capacitance between the 5022 grid, the 6L6 plate, and ground. These leads must be short, and of large conduction area and small inductance since  $\frac{di}{dt}$  has a very large value during the pulse rise time so that the  $L \frac{di}{dt}$  voltage will be large unless L is kept sufficiently small.

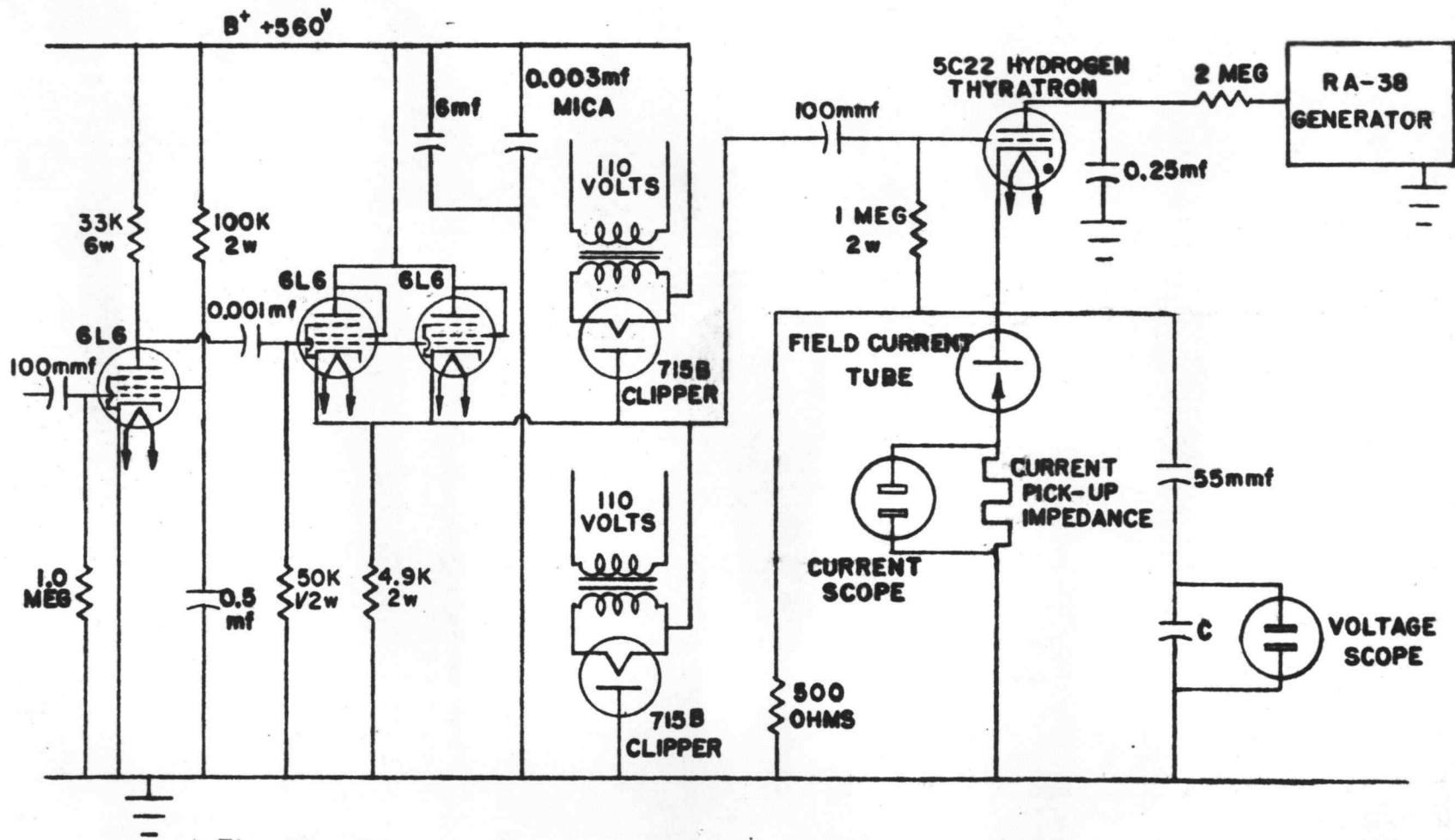


Fig. 10 Schematic diagram of trigger amplifier and pulse generator.

The 0.25 mfd. capacitor of the pulse generator is charged through a resistance of 2.0 megohms. The charging time constant is 0.5 second. During the discharge time the 2.0 megohm resistor acts like an open switch effectively preventing recharging of the capacitor during this period. The 5C22 hydrogen thyatron is capable of withstanding and switching 16,000 volts, and can pass peak currents up to 325 amperes. The pulse rise time, limited mainly by the thyatron breakdown time, is of the order of tenths of microseconds. Figure 11 is a photograph of the pulse generator.

#### Voltage Dividers

The voltage pulse must be reliably recorded on the oscillograph without distortion of any type. Since this voltage is large it must be accurately divided to a value suitable for application directly to the deflector plates of the oscilloscope. Three convenient types of voltage dividers are applicable. One is the straight capacity divider represented in Fig. 12a. Figure 12b shows a straight resistance divider; Fig. 12c a balanced RC divider. Fig. 12d is an unbalanced RC divider which may produce distortion. Any of the three dividers, a, b, or c will present a true picture of the voltage pulse but, unfortunately, types a and b become unbalanced when adapted for use directly on the deflector plates of the oscilloscope because of the capacitance between the deflector plates and the connecting leads. The capacity divider becomes unbalanced because of the necessity of placing a resistance in parallel with the deflector plates in

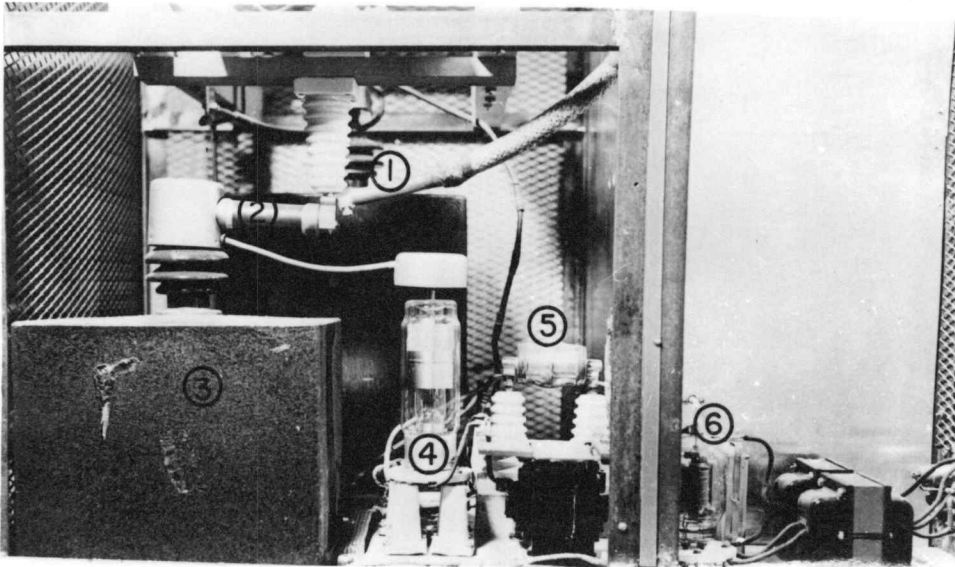
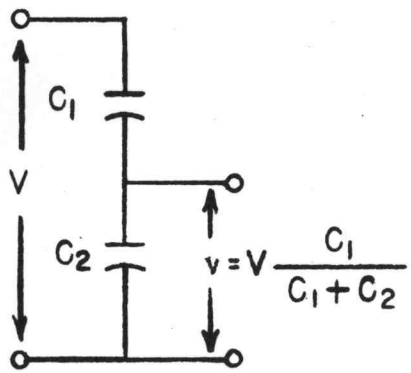
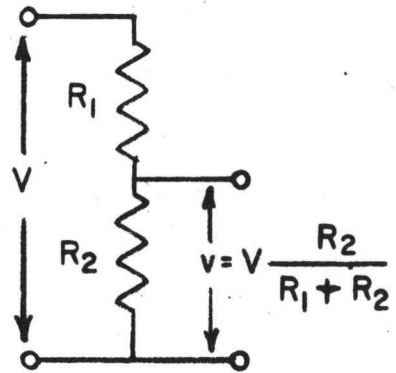


Fig. 11 Pulse Generator

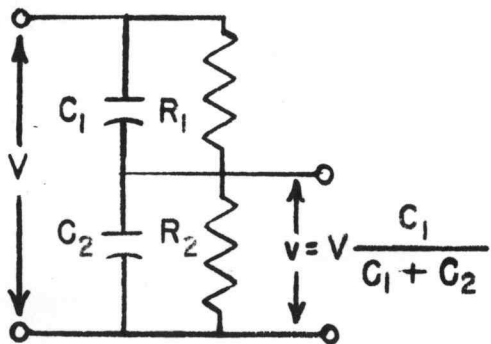
1. High voltage cable terminal from RA-38 DC generator.
2. Two megohm resistor.
3. Pulse generator storage capacitor.
4. 5C22 Hydrogen thyratron.
5. Vacuum capacitor.
6. 715 B clipper tube.



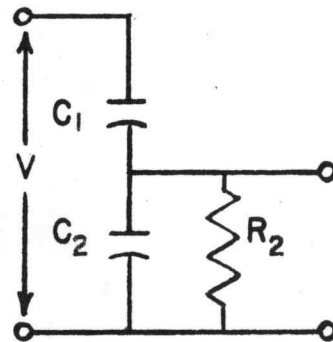
a.



b.



c.



d.

Fig. 12 Various types of voltage dividers.

order to provide a ground reference voltage for spot centering and focusing. The error introduced in the latter case is negligible when the time constant  $R_2 C_2$  of Fig. 12d is large compared to the period of the pulse. In the actual recording circuit  $R_2$  is chosen large. Capacitor  $C_2$  must also be large in order to accommodate the large division voltage ratios which are necessary for viewing high voltage pulses. In this case the error introduced will be negligible.

The divider actually used consisted of a 50 micromicrofarad vacuum capacitor,  $C_1$ , and a mica capacitor  $C_2$  whose value is chosen to give a proper division ratio for a normal oscilloscope deflection. The small capacitor  $C_1$  must withstand pulse voltages up to 16,000 volts.

#### Current Pick-up Devices

In order to measure the current through the field current tube a current pick-up impedance is connected in series with the tube as shown in Fig. 8. When the voltage pulse is applied to the tube, field-current is produced which flows through the current pick-up impedance producing across it a voltage that has a known relationship to the current through it. This voltage is applied to either the deflector plates, or the amplifier, of the current indicating oscilloscope.

The simplest type of impedance is a resistance. Since the voltage developed across a resistance is directly proportional to the current, the use of a resistance as a current pick-up impedance

places a rather severe limitation on the readable ratio of maximum to minimum current for each pulse. This is because of the width of the trace of the oscilloscope relative to the total available deflection. Ratios as high as 30/1 can be read with reasonable accuracy. Thus each pulse when plotted on a  $\log_e i$  graph will produce a curve which is undesirably short. It is advantageous to increase the ratio of measureable maximum to minimum current. This is possible by using a non-linear current pick-up device. Investigation of such possible devices led to the selection of crystal semiconductors similar to those used in U.H.F. detection devices. Radar crystals of the LN21 series are useable for currents ranging from a few microamperes to two or three milliamperes. Figures 13 and 14 are typical crystal calibration curves. A ratio of maximum to minimum current of about 1000/1 produces voltage ratios of about 30/1 when a crystal is used. Crystals when properly calibrated serve quite satisfactorily and increase the presentable current range by a factor of 30.

Crystals have a tendency to burn-out when subjected to excessively high currents. High current crystals such as the LN34 are capable of passing pulse currents of the order of tenths of amperes. Furthermore several LN34 crystals can be used in parallel for currents in the ampere region. It is necessary to make d-c and pulse calibration checks of all crystals before, and during, use as pick-up devices in order that any variation in their characteristics can be noted. Figure 15 shows calibration curves for several

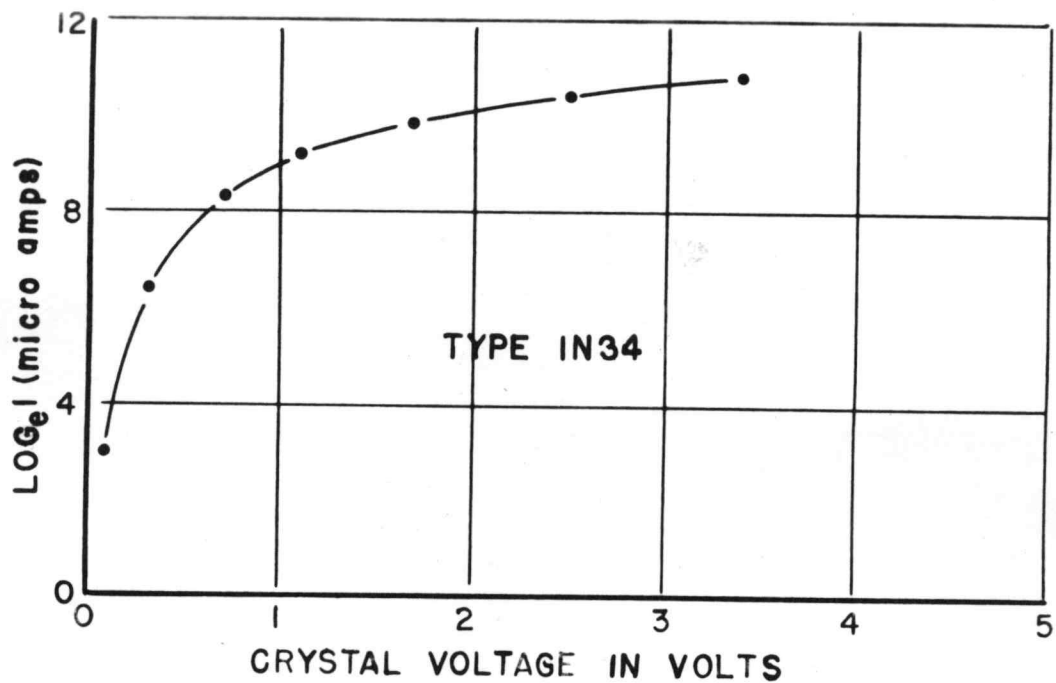


Fig. 13 Type 1N34 crystal curves.

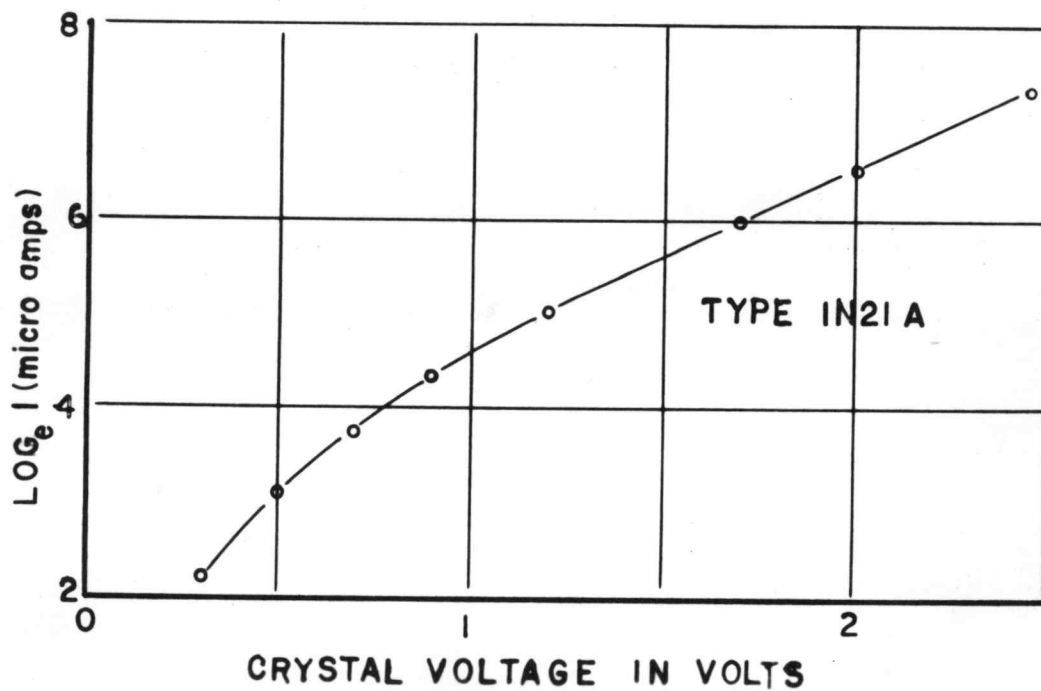


Fig. 14 Type 1N21A crystal curves.

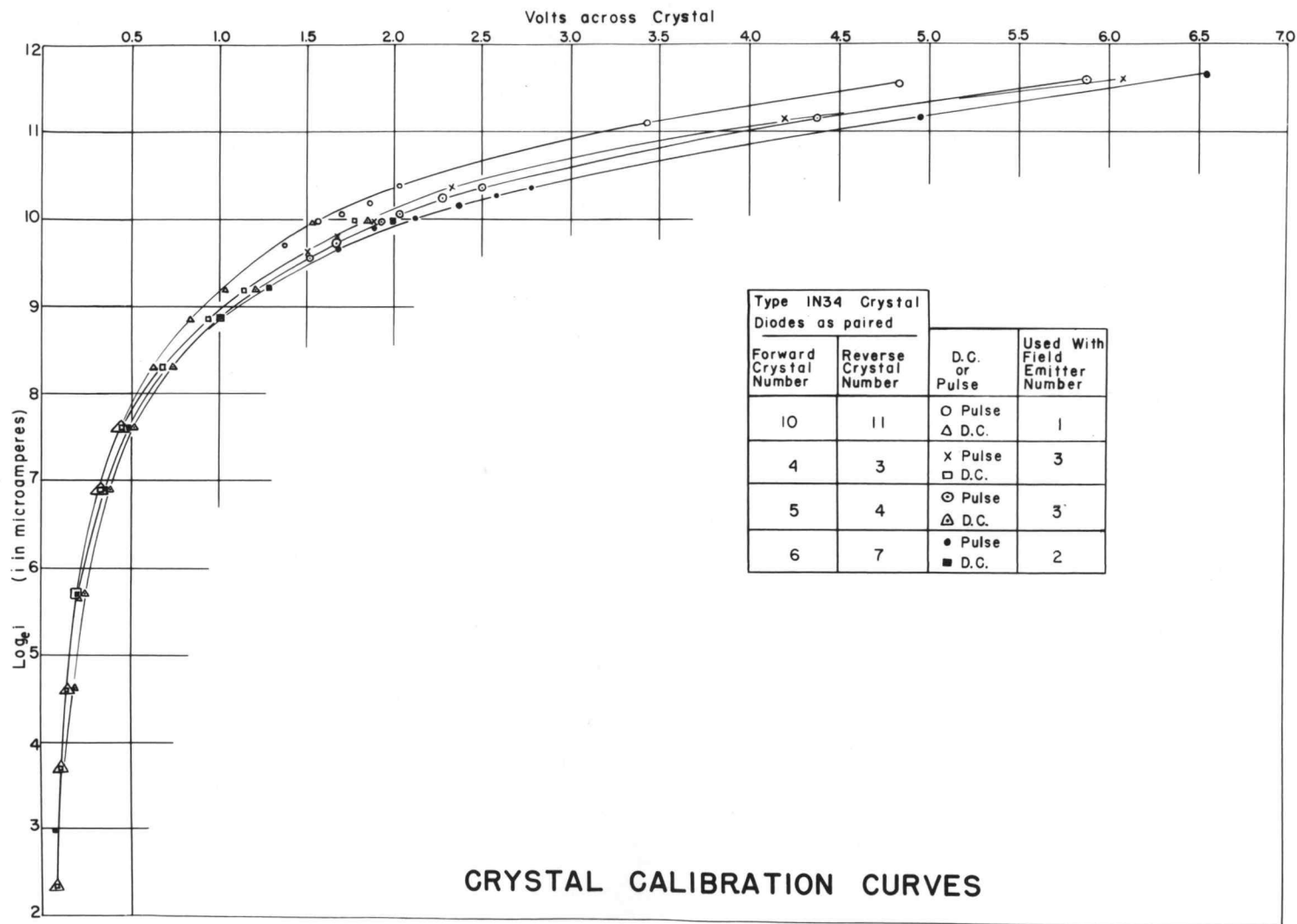


Fig. 15 Direct current and pulse calibrations of type 1N34 crystals.

LN34 crystals for both continuous and pulsed current. The use of LN34 crystals has permitted ratios of maximum to minimum pulse currents as high as 140 to 1. This is less than expected because of the adverse effects of stray capacitance in the measuring circuit. It is planned to utilize the non-linear characteristics of Thyrite for future higher current work.

### Photographic Recording

The voltage and current pulses presented on the two oscilloscopes were recorded photographically. Since these pulses were between 5 and 30 microseconds in length they posed a rather difficult photographic problem. However the use of oscilloscope tubes having fluorescent screens that emit predominantly blue light and which have 3,000 volt accelerating potentials, together with high speed Linagraph-pan film and D-19 high contrast developer, makes it possible to photograph single sweep oscilloscope writing speeds of about one inch per microsecond.

In the early part of the work the recording was done with two 4 x 5 view cameras equipped with f 2.7 Aeroektar lenses. Super XX film was used. Later two automatic 35 mm. Fairchild radar recording cameras with f 2.3 lenses were employed. The latter cameras have clock and data recording chambers which are photographed at each pulse. This is convenient in keeping exact data records.

### Experimental Tubes

Experimental tubes of several different designs have been used. A simple type, shown in Figs. 16 and 17, consists of a very sharp point emitter placed near a plane anode surface. Provision was made for heating the metals sufficiently to outgas them. The anode was bombarded by electrons supplied from an auxiliary filament located near it on the side opposite the point. The point is mounted on a horseshoe-shaped tungsten filament which can be heated by a current. Tubes of this type permit the development of high field intensities at relatively low voltages.

An emitter incorporating a single sharpened point may be subject to damage due either to positive ion bombardment, or to resistive heating, if the current densities during field emission are high. The result is that the point becomes dull and ceases to emit at available voltages. This necessitates the removal of the experimental tube from the vacuum system, and the replacement of the point emitter. In order to obtain more data per tube replacement a tube containing five points, Figs. 18 and 19, was constructed. The large cylindrical anode approximates a plane surface in the vicinity of each emitter. This anode was outgassed by bombardment with electrons supplied by a spiral tungsten filament placed inside the anode for this purpose. Each emitter point was mounted on its own filament loop for outgassing purposes. Such tubes furnished the major portion of the data taken.

Valuable data can be gathered from a tube which is similar to

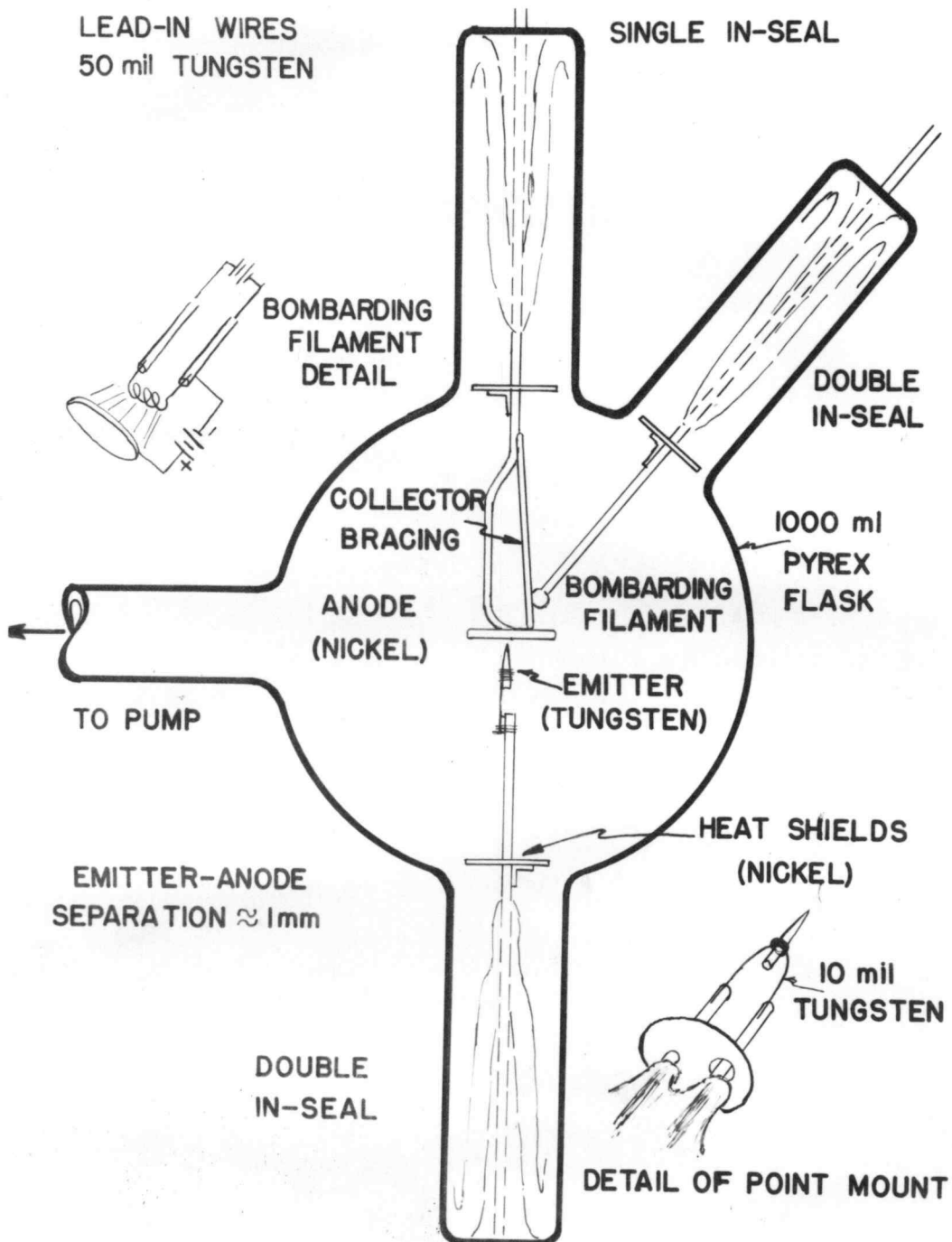


Fig. 16 Point to plane field current tube.

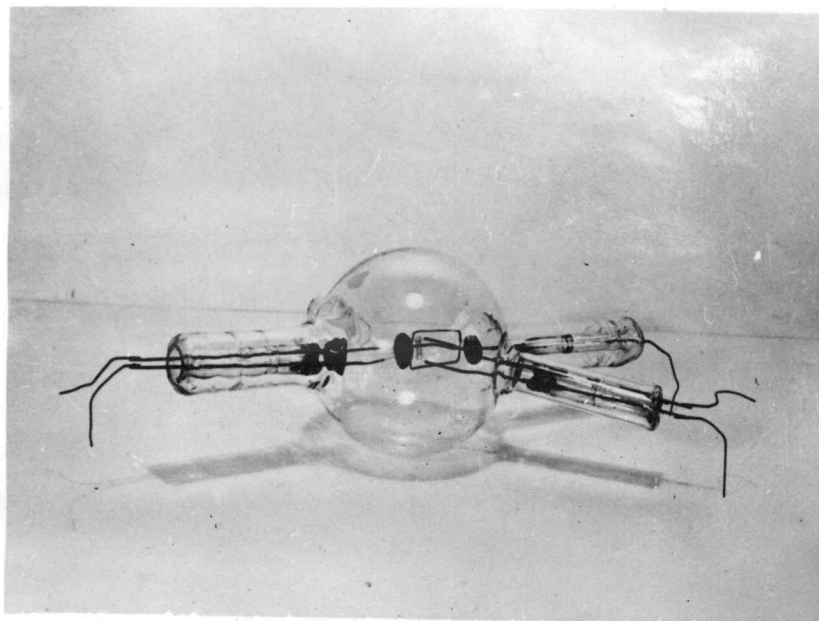


Fig. 17 Point to plane field current tube.

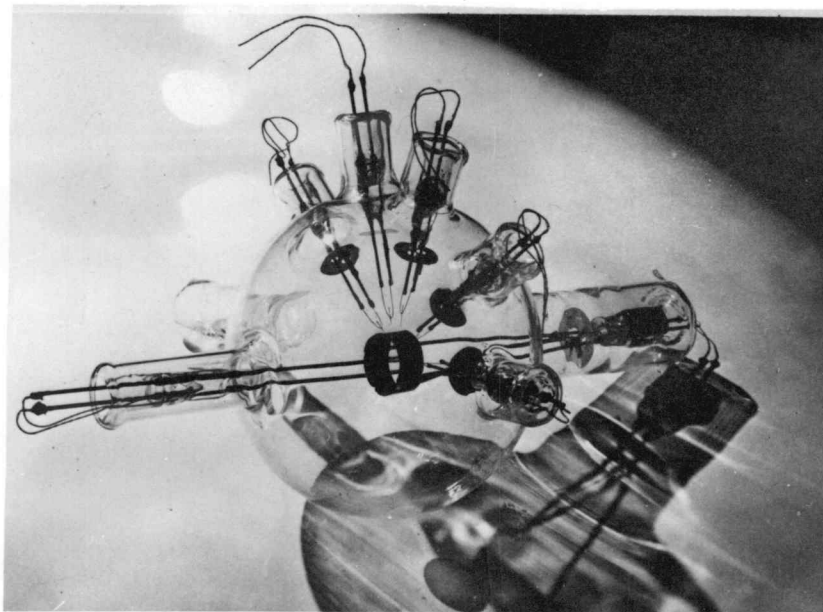


Fig. 18 Five point field current tube.

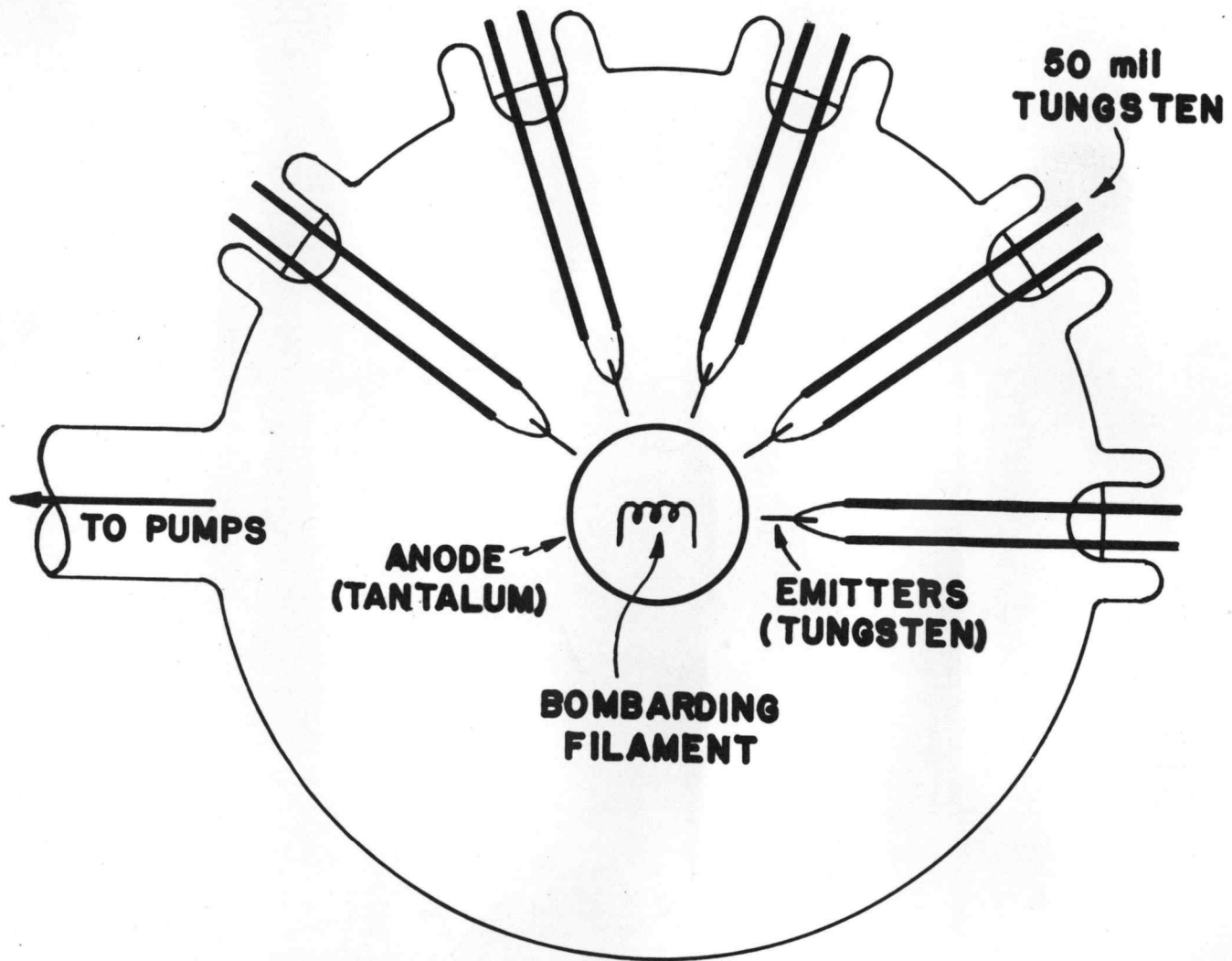


Fig. 19 Five point field current tube.

the electron microscope type of field emission tube used by Muller,<sup>11</sup> and pictured in Figs. 20 and 21. The tube envelope is a two liter Pyrex flask with a coating of willemite over one-half of the inner surface of the sphere. The anode is a ring-shaped piece of tungsten wire located near the center of the sphere. The emitter, placed near the anode, is a sharp tungsten point. This type of tube is referred to as a projection tube or an electron microscope tube. The emitted electrons diverge and strike the willemite screen causing it to fluoresce. The pattern on the willemite screen is an enlarged projection of the emission pattern of the point and shows the detailed distribution of the emission at the surface of the emitter. Such patterns have been observed under both direct current and pulse conditions.

A tube utilizing a linear filament and cylindrical symmetry has been constructed as shown in Figs. 22 and 23. The anode is a double ended tungsten spiral 2.4 cm in diameter, 2.8 cm in length using a wire diameter of 0.015 inch. It can be heated by a current to the outgassing temperature. The linear tungsten filament is 0.001 cm in diameter and can be outgassed in a manner similar to that used for the anode. The inner glass surfaces are dusted with willemite which fluoresces under electron bombardment. This tube contains a comparatively small amount of metal and is therefore easily outgassed.

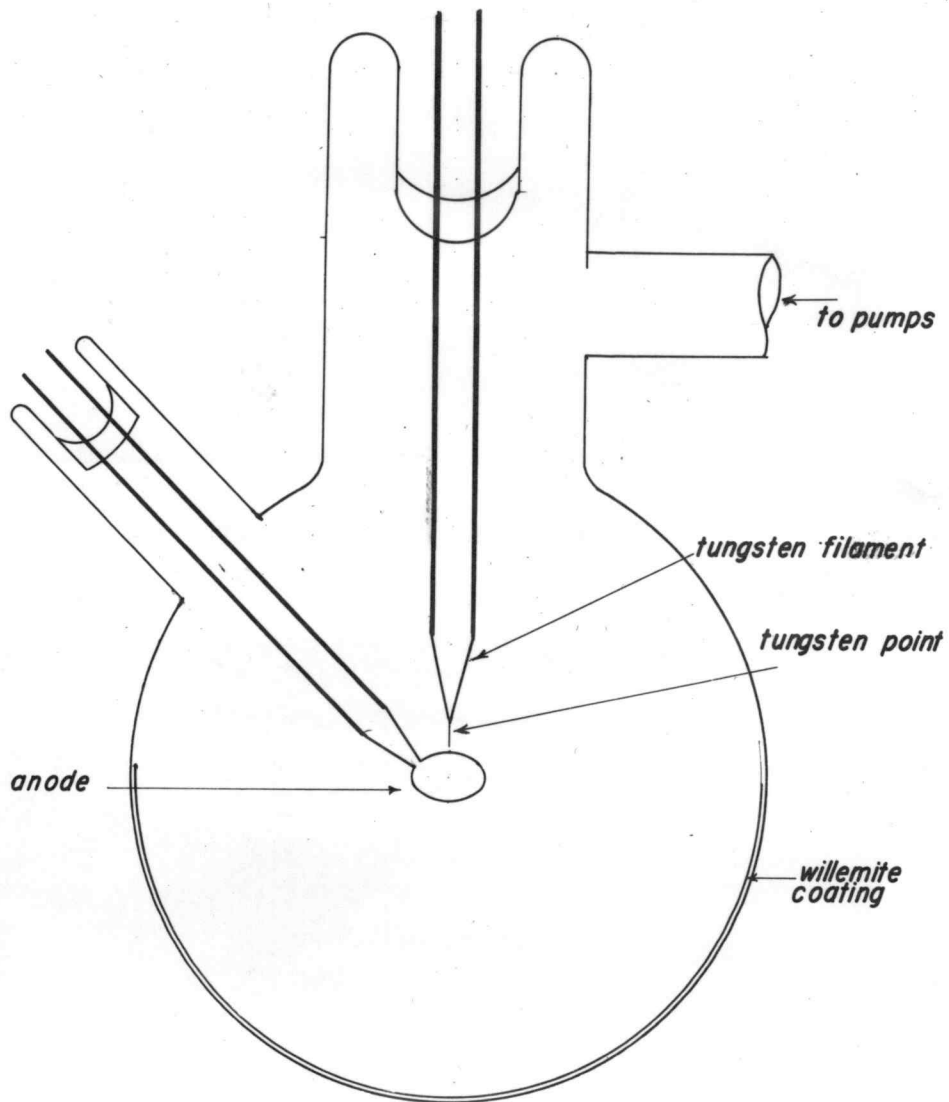


Fig. 20 Electron microscope type tube.

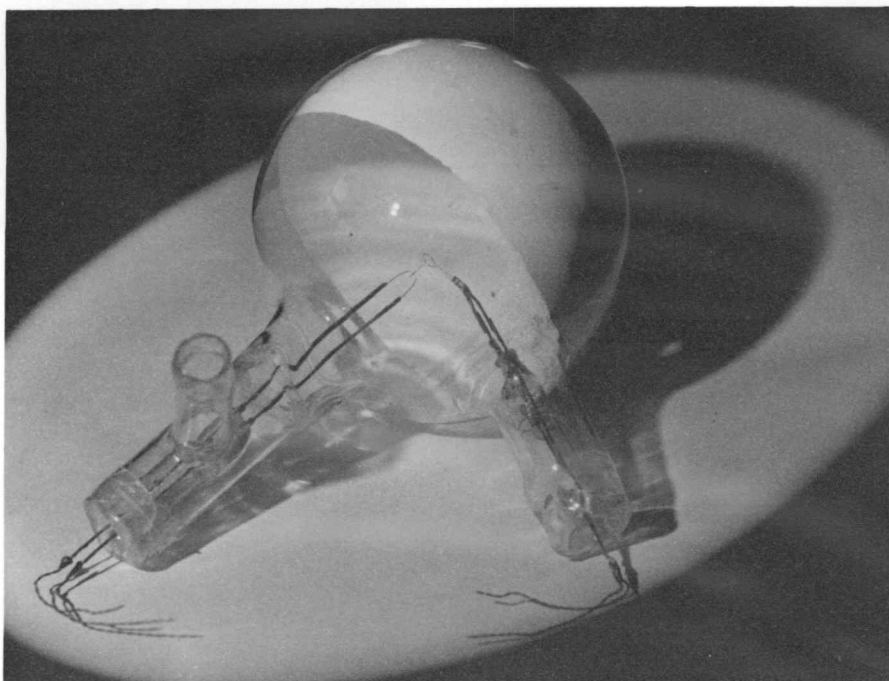


Fig. 21 Electron microscope type tube.

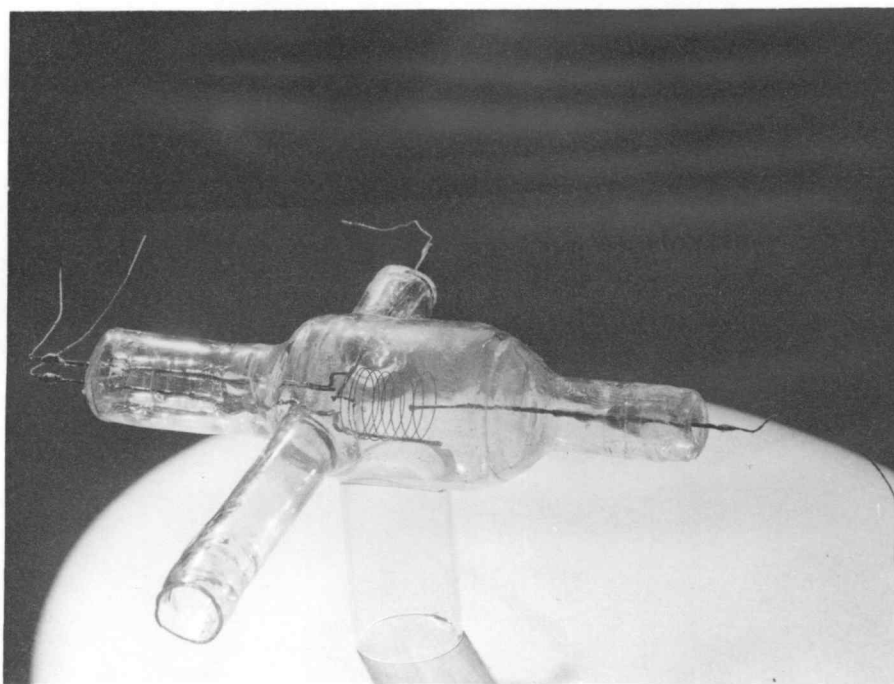


Fig. 22 Linear filament type tube.

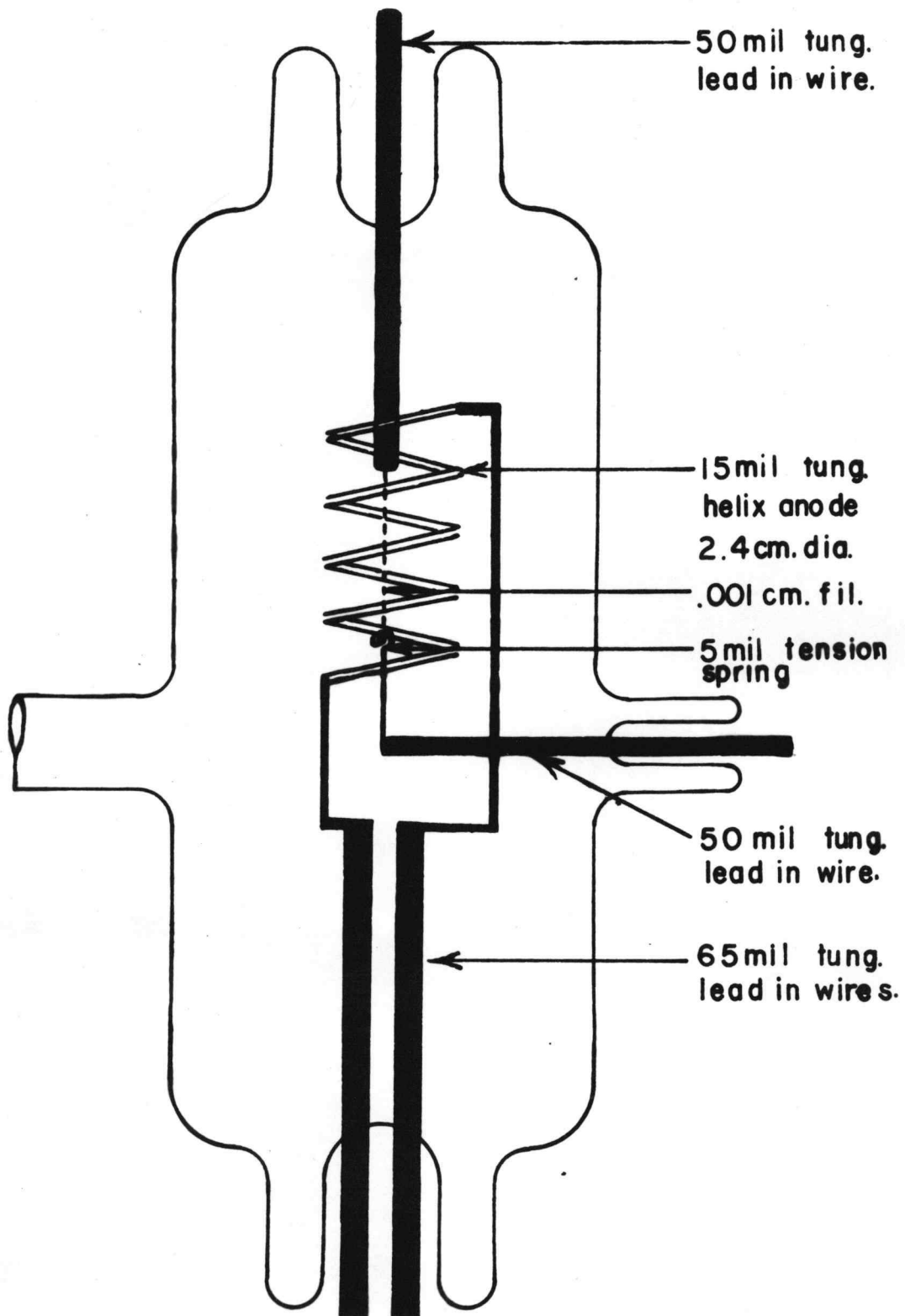


Fig. 23 Linear filament type tube.

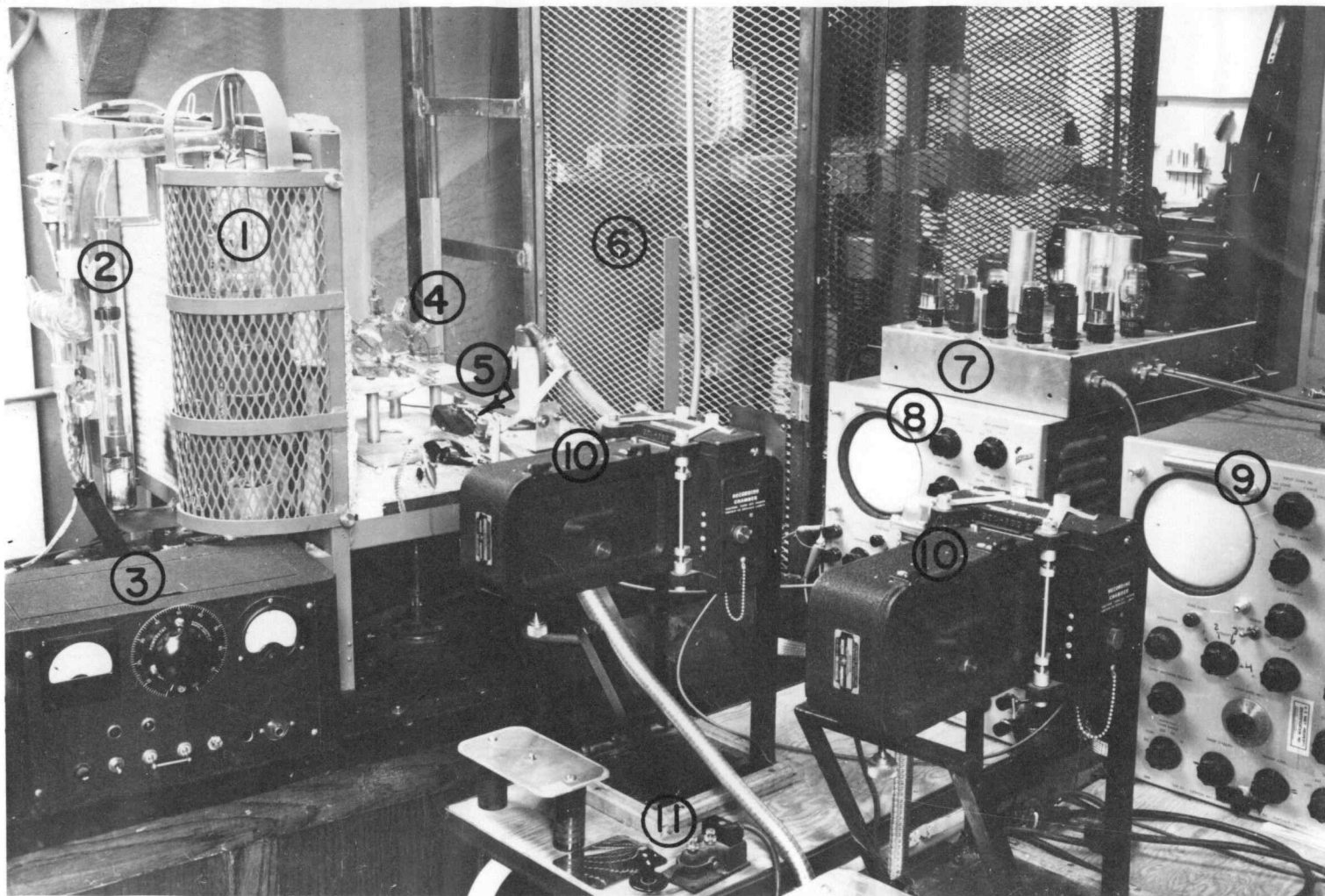


Fig. 24 Arrangement of equipment for data run.

## KEY TO FIG. 24

1. Oil diffusion pump.
2. Oil McCleod gauge.
3. Ionization gauge control.
4. Five-point field current tube.
5. Current pick-up impedance.
6. Pulse generator (inside cage).
7. Trigger and time-marker generator.
8. Current recording oscilloscope.
9. Voltage recording oscilloscope.
10. Oscilloscope recording cameras.
11. Telegraph key.

The field at the surface of the filament is expressed approximately by

$$F = \frac{1}{a} \frac{V}{\log_e \frac{b}{a}}$$

where  $a$  is the radius of the filament,  
 $b$  the radius of the anode and  
 $V$  the applied voltage.

This indicates that a thin filament is necessary in order to obtain an intense electric field in its vicinity. Extreme difficulty was encountered in establishing a filament of the proper dimensions and in mounting it to withstand the mechanical shock of the pulse voltage.

### Calibrations

All devices used for determining voltage and current must be carefully calibrated. To this end all measurements were referred to one scale of a standard d-c voltmeter and to a General Radio Impedance Bridge.

Voltage oscilloscope calibration consists of applying known d-c voltages to the oscilloscope plates to deflect the base line and photographing these deflections with the recording cameras. Although the base line appears as a straight line when located at the center of the oscilloscope it is curved when deflected above or below the center of the tube. This distortion tends to bow the ends of the trace toward the center line. Although corrections for this can be determined from the calibrations most of the data are taken from the center of the scope face and thus suffer no significant distortion.

The sensitivity of the current indicating oscilloscope was determined by applying various known a-c voltages to the oscilloscope amplifier input and recording the resulting deflections photographically. The sensitivity is expressed in terms of voltage per millimeter of deflection.

To determine the voltage division ratio of the capacitance divider each capacitor, while in its operating position, was measured by means of the General Radio Impedance Bridge. The voltage division between two capacitors in series was then calculated in the usual manner. Finally the capacity divider and the oscilloscope deflection which it caused were checked by applying a known d-c voltage to the divider by means of a vacuum switch.

The current-voltage characteristic of each current pick-up crystal was obtained from direct current measurements of the voltage across the crystal and the current through it. This calibration covered current ranges from a few microamperes to about 30 milliamperes. In order to extend the calibration curve to large currents, a known voltage pulse was applied to each crystal in series with a known resistance. The voltage across the crystal was recorded by the camera of the current reading oscilloscope while the voltage across the resistor and crystal in series was recorded on the voltage recording camera. From these two curves crystal voltage and crystal current can be found. The excellent agreement between pulse currents and d-c currents at the same voltage can be seen on the overlapping portions of the crystal calibration curves of Fig. 15.

The Leeds and Northrup type R galvanometer, used for the direct current field emission measurements, was carefully calibrated against the standard voltmeter and the impedance bridge. Its sensitivity is  $1.18 \times 10^{-10}$  ampere per millimeter at one meter.



ADVANCE BOND

W. L. BROWN Paper

## EXPERIMENTAL PROCEDURE

Field emission experiments can be successfully performed only in a vacuum equal to, or better than,  $10^{-7}$  mm of Hg. The vacuum system employed for this work consisted of a two stage, water cooled, oil-diffusion pump (11, p. 66-67) backed with a type 1405H Welch Duo-seal mechanical pump. The fore-pressure was measured with an oil McCleod gauge; the high vacuum with a Distillation Products VG-1A, or similar type ionization gauge. A total-obstruction charcoal trap was used in the pumping line on the high vacuum side and was baked out along with the tube and ion gauge. The charcoal trap, although not immersed in liquid air, trapped gas and oil vapors and effected a considerable improvement in the vacuum. Octoil S was used as the diffusion pump oil.

The vacuum system was mounted in a stationary framework with provision for lowering an oven over the high vacuum portion of the system during the baking-out period. Two thirty-ampere Variacs provided adjustment for controlling the oven temperature. During the bake-out period of five to fifteen hours, the tube, charcoal trap, and ion gauge were heated to a temperature of  $500^{\circ}\text{C}$ . After the system had cooled to nearly room temperature, clear glyptol was painted over the glass joints and seals of the tube as a precaution against minute leaks that might exist in the glass and in-seals.

Next, the metal parts were heated to appropriate outgassing temperatures by conduction, bombardment, or in an induction furnace. The temperatures were measured by means of a Leeds and Nothrup optical

pyrometer. After the metals had outgassed for several hours, the vacuum was measured, and if found satisfactory, the field current tube was put into operation.

Prior to any pulse operation, direct current runs were made to establish the relationship between current and voltage at low current densities. This initial period of operation also tended to stabilize the operating characteristics of the emitters. Pulse data were taken by means of techniques and methods already described. Usually the pulse voltages were increased with successive pulses. Sometimes many pulse readings were made at the same peak voltage in order to see whether or not similar voltage pulses produced similar current curves. In general the procedure was determined by the trend of the visually observable results. The pulsed voltage was eventually increased to the maximum which the particular tube would stand. Experiments, or runs, were usually terminated by burning off the point, or blowing up the filament emitter, so that field emission could no longer be produced in the tube.

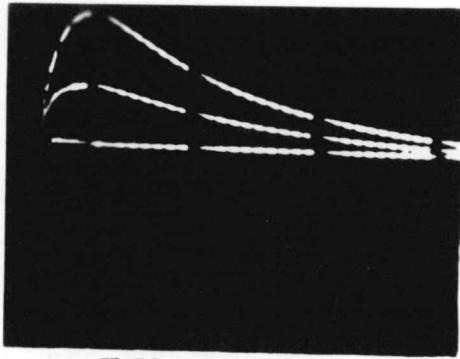
## EXPERIMENTAL RESULTS

Data from pulsed field emitters are taken from photographs of oscilloscope traces which record the voltage applied to the emitter and the current which it yields. Figure 25 reproduces typical photographs. Corresponding values of voltage and current, at any instant, are determined from measured deflections on the photographic image, following the procedure outlined previously in the discussion of the methods of calibration. A graph of  $\log_e i$  versus  $10^4/\sqrt{V}$  for four pulses from a typical emitter is shown in Fig. 27. The excellent reproducibility of the data, which Fig. 27 indicates, is typical of the pulsed emitters which have been studied, with a few significant exceptions which will be noted later.

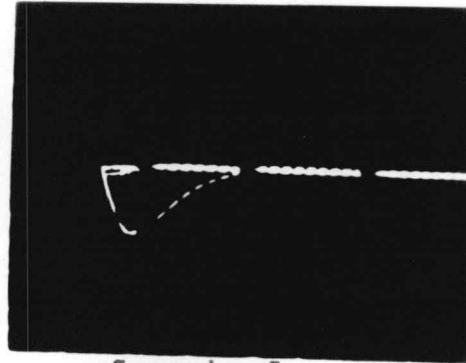
Data from the same field emitters when used as sources of continuous direct current emission are also plotted as  $\log_e i$  versus  $10^4/\sqrt{V}$ . In Figure 26, which is typical, this relationship is found to be linear. Direct currents in the range  $10^{-11}$  to  $10^{-6}$  amperes were studied.

Data for both direct current and pulsed operation are combined in Figs. 28, 29, and 30 in order to describe the performance of each of three very sharp tungsten point-to-plane emitters over a wide range of emission currents. These three emitters were used in the experimental tube shown in Figs. 18 and 19.

It is possible to compare the experimental curves of Figs. 28, 29, and 30 with the theory of Fowler and Nordheim (9, p. 179) by the use of a method due to Stern, Gossling and Fowler (20, p. 699-700).



Voltage pulse



Current pulse

Fig. 25 Typical current and voltage pulses from oscilloscope photographs.

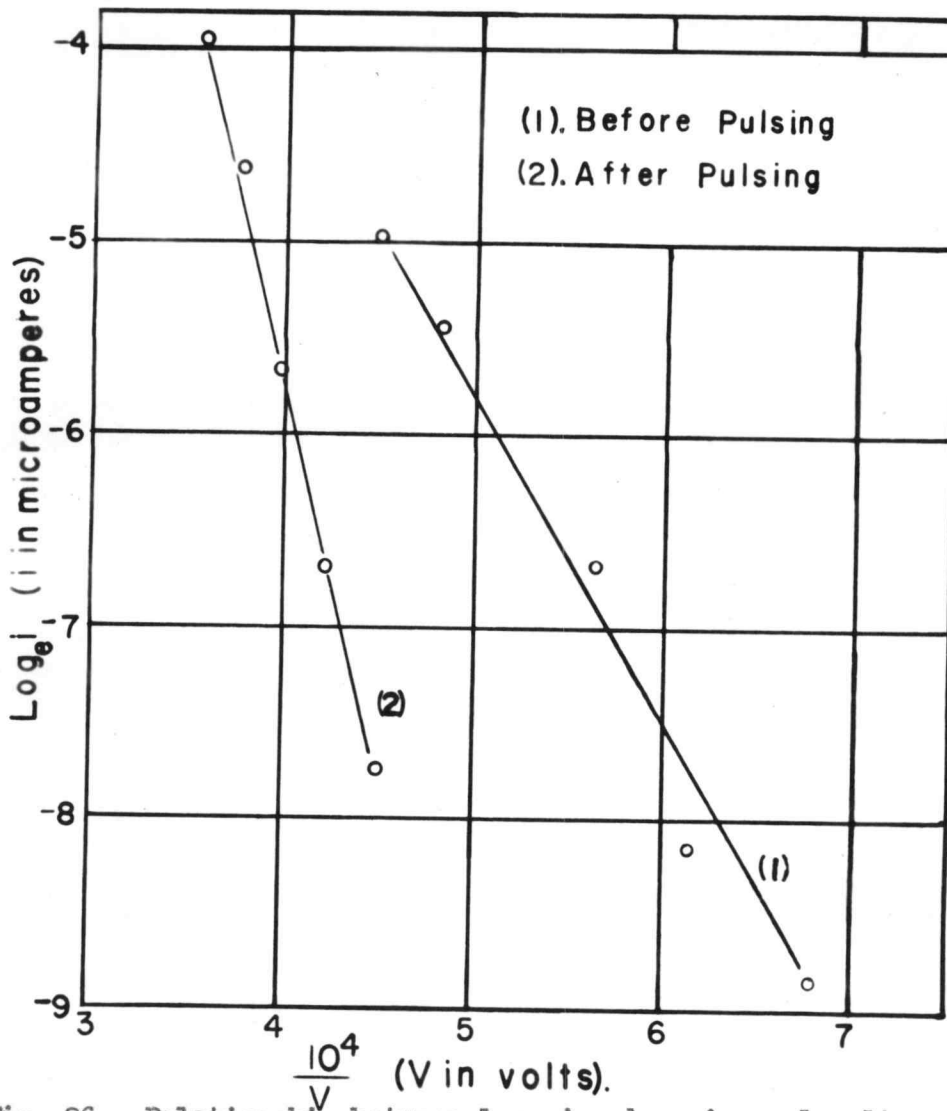


Fig. 26 Relationship between  $\log_e i$  and reciprocal voltage for a direct current tungsten field emitter.

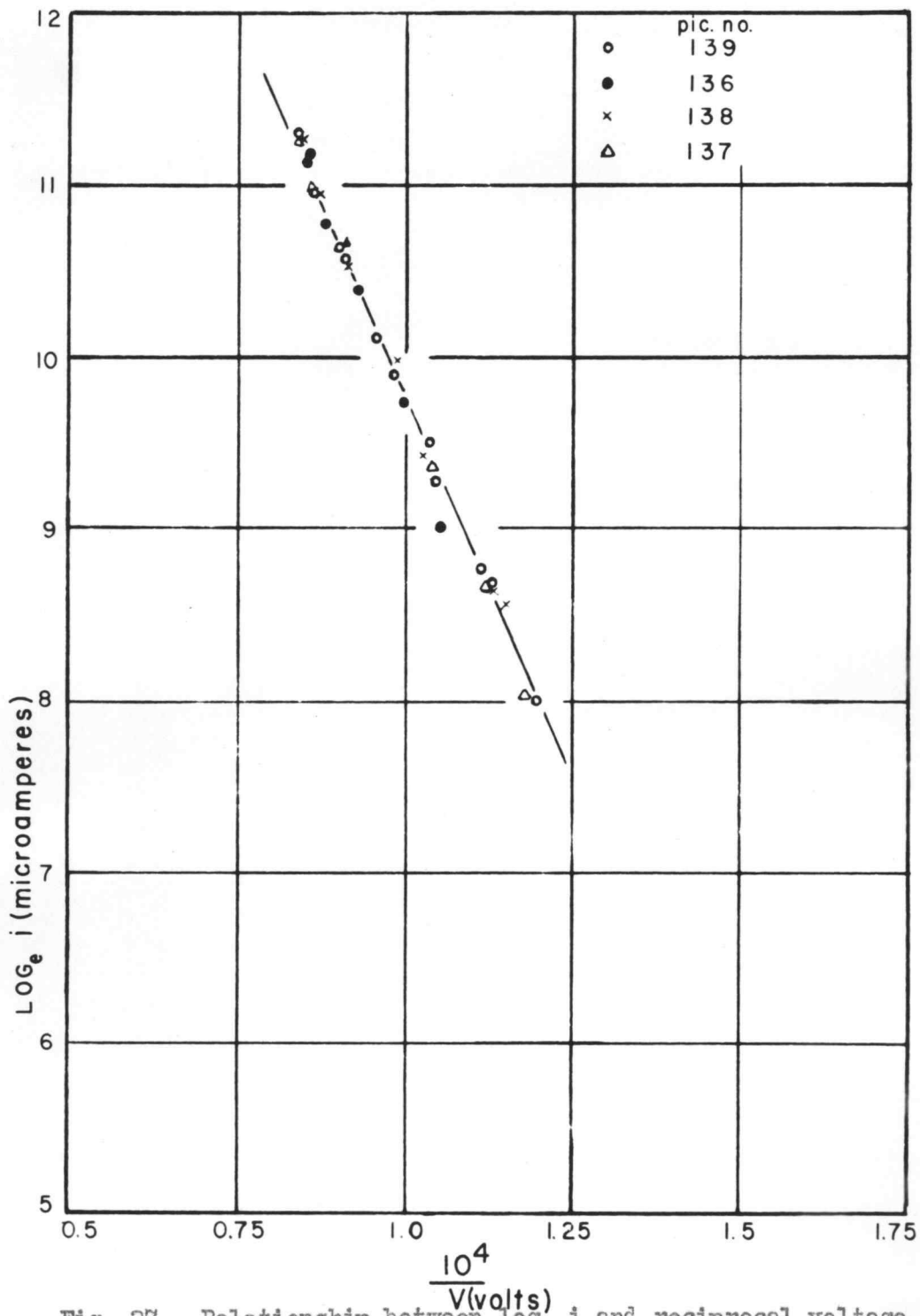


Fig. 27 Relationship between  $\text{LOG}_e i$  and reciprocal voltage showing reproducibility of data for several pulses from a single emitter.

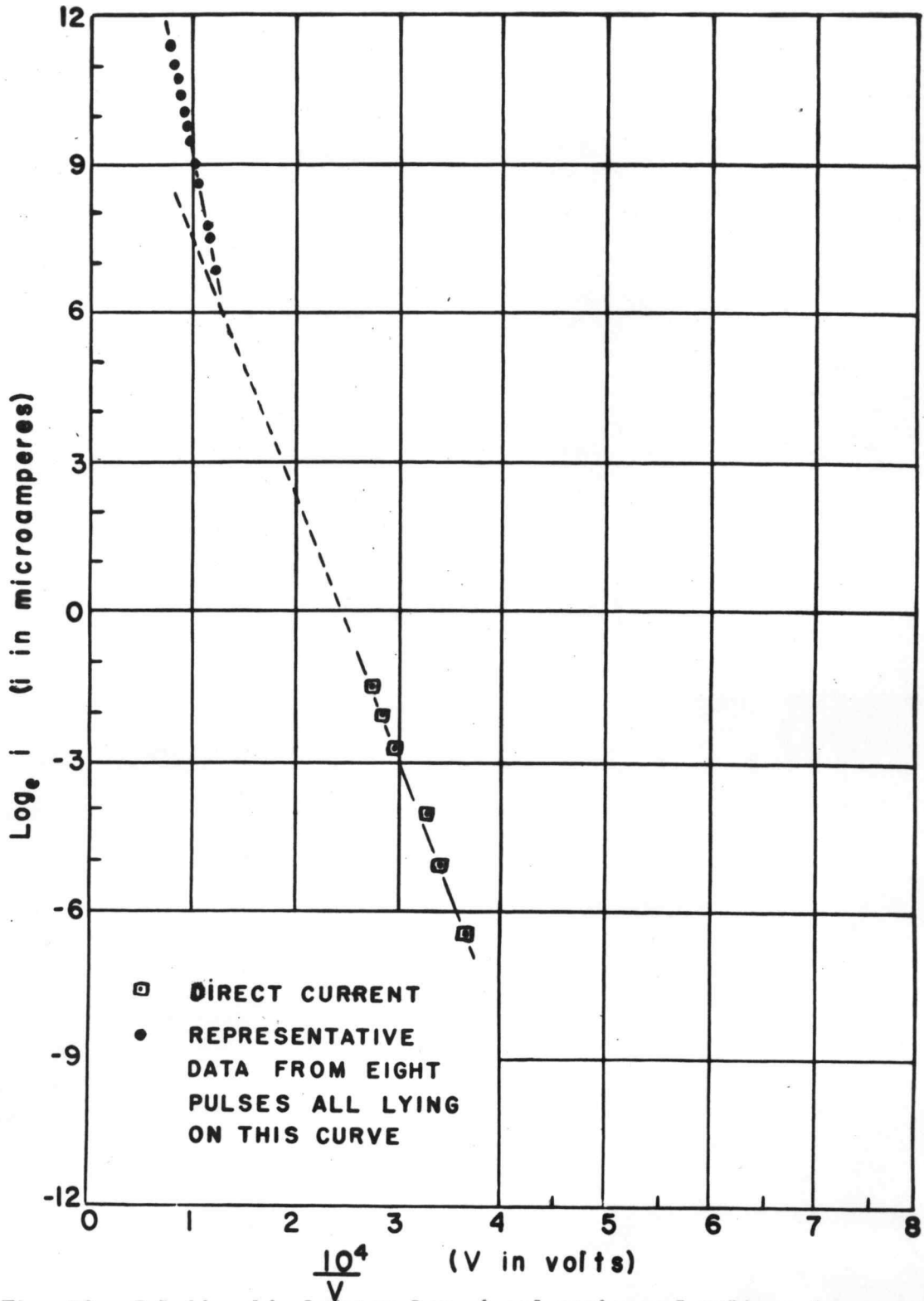


Fig. 28 Relationship between  $\log_e i$  and reciprocal voltage for field emitter #1, for both pulsed and d-c operation.

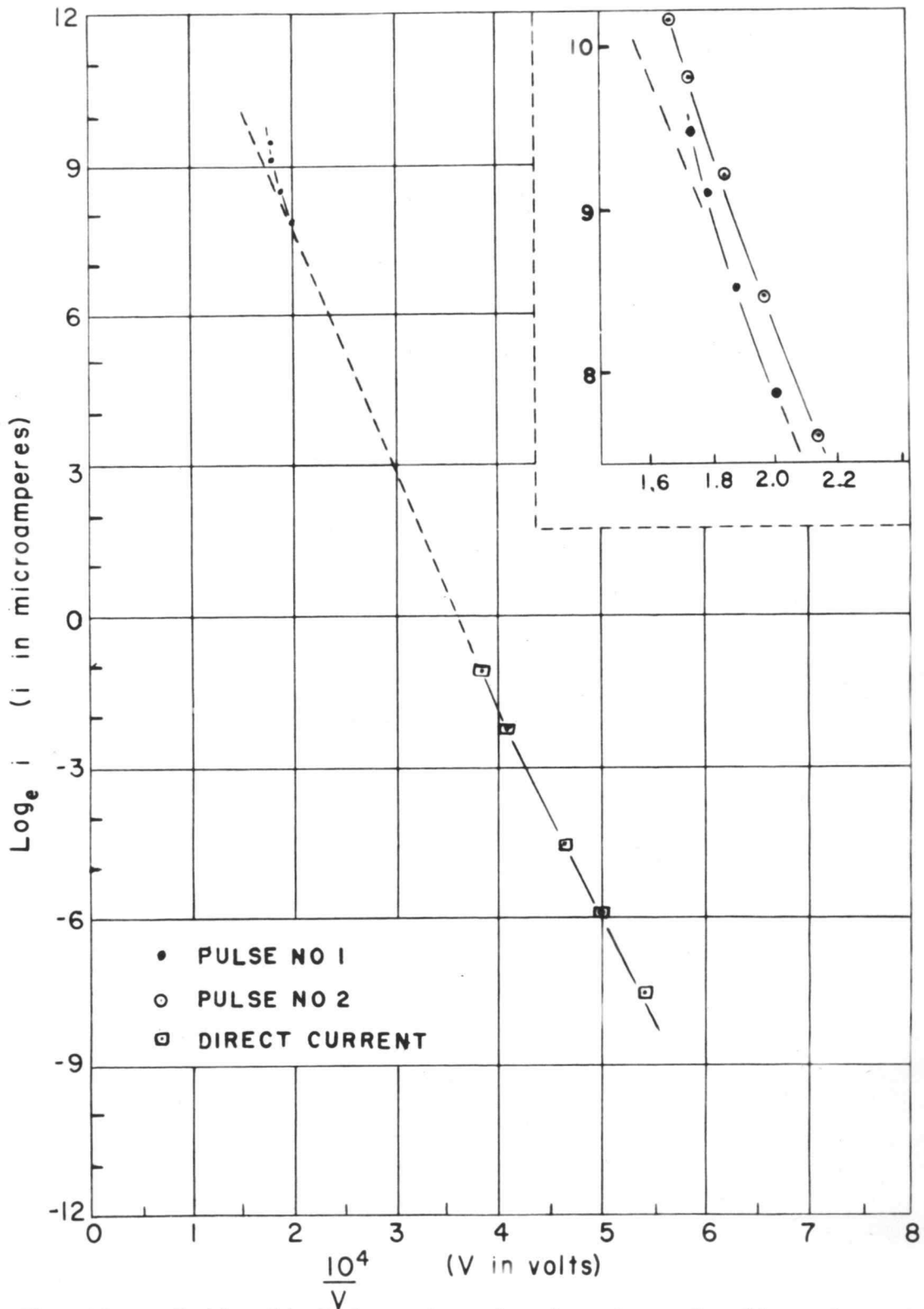


Fig. 29 Relationship between  $\log_e i$  and reciprocal voltage for field emitter #2, for both pulsed and d-c operation.

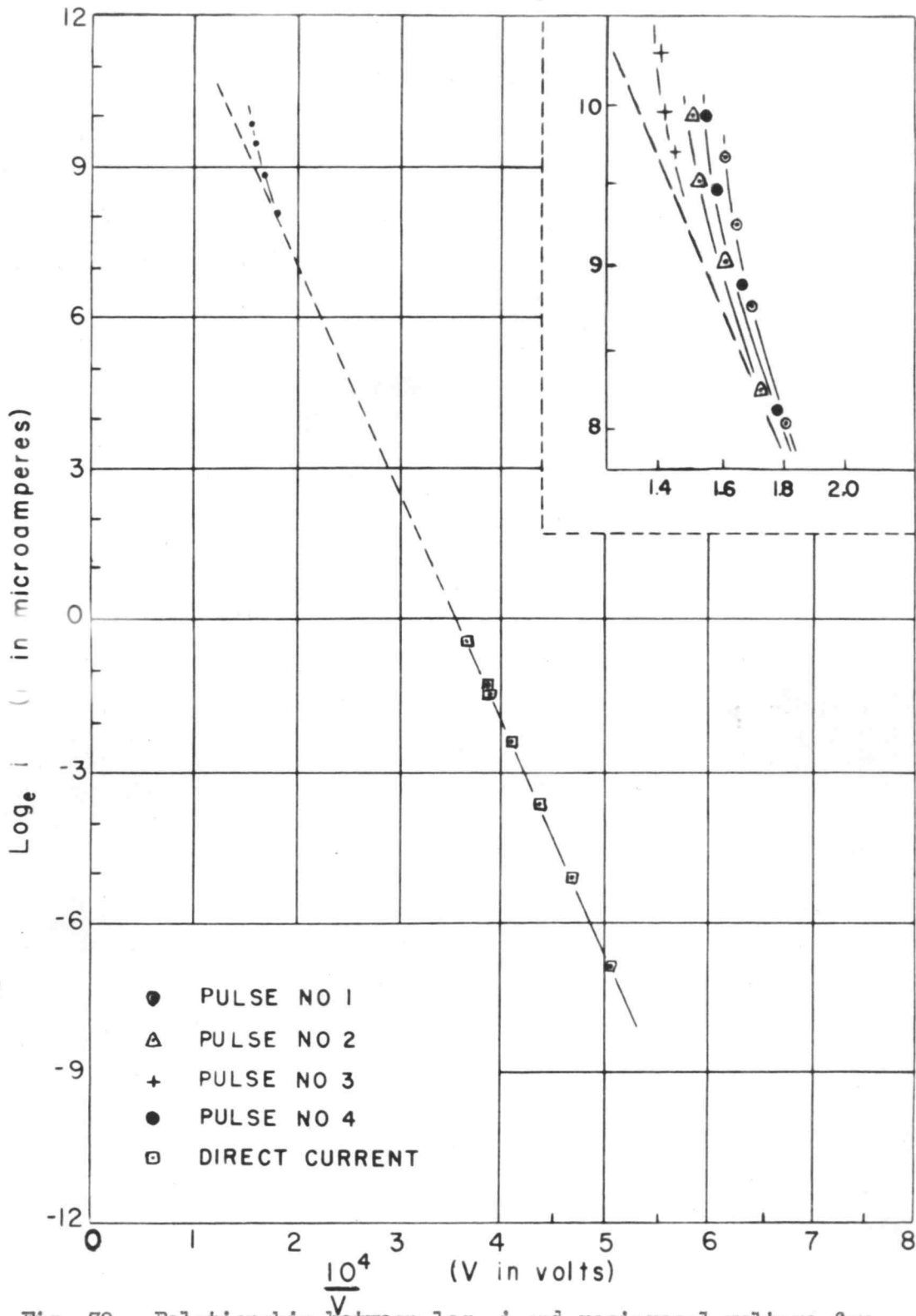


Fig. 30 Relationship between  $\log_e i$  and reciprocal voltage for field emitter #3, for both pulsed and d-c operation.

Fowler and Nordheim (9, p. 173-181) and Nordheim (17, p. 626-639) consider that there exists at the surface of a metal, a potential barrier which is the sum of three potentials. These are the roughly rectangular potential barrier due to the metal, the potential due to the applied field, and the potential due to the image force on an emitted electron. This potential distribution is shown in Fig. 6. Free electrons inside the metal may, according to wave mechanical theory, strike and penetrate the barrier. An expression for emission current density is obtained if the probability of penetration is integrated over all available electron energies taking account of the shape and height of the surface barrier.

Fowler and Nordheim find the density of this field current to be

$$J = 6.2 \times 10^{-6} \frac{\mu^{\frac{1}{2}} F^2}{(\phi + \mu)\phi^{\frac{1}{2}}} e^{-\frac{6.8 \times 10^7 \phi^{\frac{3}{2}}}{F}} f(y). \text{ Amperes/cm.}^2$$

where  $F$  = electric field in volts/cm.,

$\phi$  = metallic work function in electron volts,

$\mu$  = the usual metallic parameter (see Fig. 6),

$$f(y) = \sqrt{\frac{1 + \sqrt{1-y^2}}{2}} \left[ E(k) - \frac{y^2}{1 + \sqrt{1-y^2}} K(k) \right]$$

$$y = \sqrt{\frac{eF}{\phi}}, \quad k = \frac{2\sqrt{1-y^2}}{1 + \sqrt{1-y^2}}$$

$$K(k) = \int_0^{\frac{\pi}{2}} (1-k^2 \sin^2 \theta)^{-\frac{1}{2}} d\theta$$

$$E(k) = \int_0^{\frac{\pi}{2}} (1-k^2 \sin^2 \theta) d\theta$$

This theoretical equation is plotted for values of the work function  $\phi = 3$ , and  $\phi = 4.5$  volts in curves 9 and 7 respectively,

Fig. 31. A third curve is drawn from theory under the assumption that  $f(y) = 1$  (curve 8, Fig. 31). This is the earlier theoretical curve from the original work of Fowler and Nordheim (9, p. 173-181). It neglects the contribution of the image force to the surface potential barrier. It is the latter curve which Stern, Gossling and Fowler used in their comparison between experiment and theory. A slight modification in their method permits a comparison of the experimental data of Figs. 28, 29, and 30 with the most recent theory of Fowler and Nordheim (9, p. 173-181), (17, p. 626-639).

Consider first curve 8 of Fig. 31. The departure from linearity in the plot of  $\log_e i$  versus  $10^8/F$  is detectable only at very large fields. The effect of the image force, i.e.,  $f(y)$ , is two-fold and accounts for the difference between curves 8 and 7. First,  $f(y)$  causes curve 7 to be offset in the direction of higher current densities and second, the departure from linearity becomes observable at somewhat lower values of the electric field.

An examination of the form of  $f(y)$  shows it to be approximately equal to unity at fields lower than those for which detectable curvature sets in. Values for  $f(y)$  are given by Nordheim (17, p. 638) and are reproduced in Table 1.

TABLE 1

$y$	0	0.2	0.3	0.4	0.5	0.6	0.7	0.8	0.9	1.0
$f(y)$	1	0.951	0.904	0.849	0.781	0.696	0.603	0.494	0.345	0

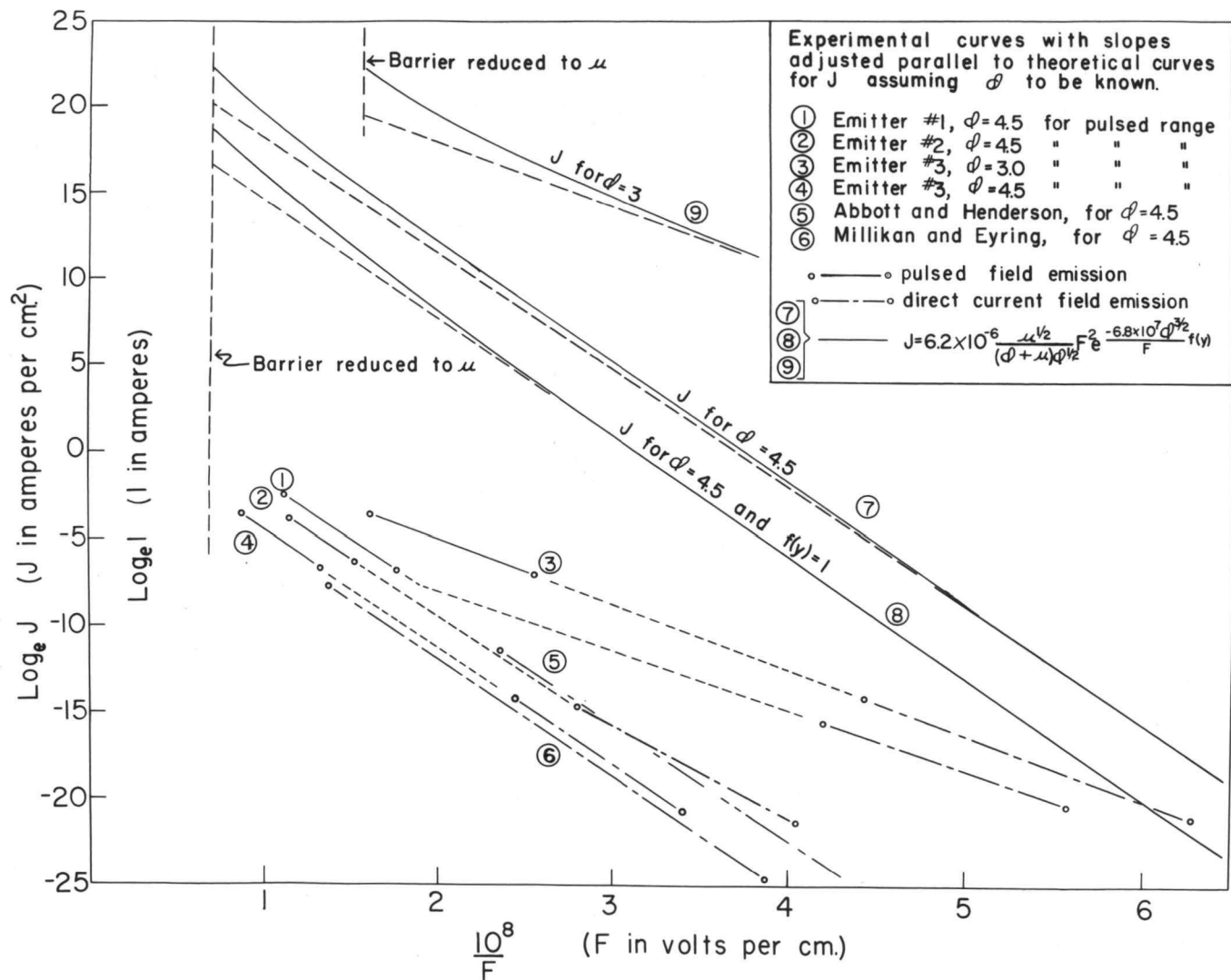


Fig. 31 Graph of  $\log_e i$  versus reciprocal voltage showing comparisons of experimental curves with theoretical curves.

where  $y = \frac{3.78 \times 10^{-4}}{\phi} \sqrt{F}$  ,       $F$  is expressed in volts/cm  
 $\phi$  is expressed in volts.

When the surface barrier of the metal is reduced by the amount  $\phi$  to the level  $\mu$ , (Fig. 6)  $f(y)$  is reduced to zero. This occurs for  $F = 1.42 \times 10^8$  volts/cm if  $\phi = 4.5$  volts, the accepted value of the thermionic work function of tungsten. The theory of Fowler and Nordheim extends to this limit, which is indicated by the vertical dashed line which terminates curve 7, in Fig. 31. This limit is reached at somewhat lower values of field when  $\phi = 3$  as shown in curve 9, Fig. 31.

A comparison between experiment and theory amounts to a determination experimentally of the three unknowns,  $F$ ,  $J$  and  $\phi$ . Experimental values for the electric field do not usually agree exactly with theoretical values. Careful studies (13, p. 52-67) (20, p. 699-723) (1, p. 113-118) (17, p. 626-639) have shown that field emission occurs at measured electric fields which are found to be from 1/2 to 1/100 as large as expected from theory. A current of  $10^{-11}$  amperes from very sharp emitters usually requires a measured electric field of the order of  $10^6$  volts/cm. Theoretical values for the fields are considered to be correct, and the disagreement with experimental values is attributed to sub-microscopic projections or minute spots of impurities which experiment has not as yet detected.

Fortunately, the work function  $\phi$  has been determined experimentally, by methods independent of field emission, and is known for metallic emitters whose surfaces are clean and well outgassed.

The relationship between the emission current density  $J$ , the emitting area  $A$  and the total emitted current  $i$  has been investigated experimentally by Müller (16, p. 541-550) using an electron microscope technique which permitted the emission pattern, enlarged by a factor of  $2 \times 10^5$ , to be viewed on a fluorescent screen. From this work the values of  $J$  and  $A$  have been determined, with precision, under actual operating conditions. Müller used a very sharp tungsten emitter formed by electrolytically etching the end of a wire in sodium nitrite. The importance of Müller's work is apparent since it determines accurately the variables  $J$  and  $A$  under the experimental conditions used. Hence with  $\phi$  known, and  $F$  known within reasonable limits, a check on the order of magnitude of the theoretical equation can be made using emitters similar to Müller's.

The emitters used in the present work are very sharp tungsten points prepared by electrolytic etching in sodium hydroxide, which is considered equivalent to the method used by Müller. In order to obtain sufficiently large current densities, using the potential source available, it was necessary to achieve maximum field strength at the emitter by forming it into a very sharp point. This precluded the possibility of determining experimentally the applied electric field since the points were so sharp that only an electron microscope could be expected to resolve them. The electric field was determined, therefore, from the theoretical equations assuming  $\phi$  to be known. This method is sufficiently accurate to permit an order-of-magnitude comparison between experiment and theory and thus permits an

approximate calculation of  $J$  and  $A$  for the emitters used. The values thus obtained are close to those observed by Müller under similar conditions.

To determine the electric field  $F$ , current density  $J$ , and emitting area  $A$ , as described above, it is only necessary that  $\phi$  be known, and that the experimental curves in Figs. 28, 29 and 30 be replotted with slopes parallel to those of the theoretical equations for  $J$  when these are plotted with the known value of  $\phi$ . This is done in Fig. 31, curves 1, 2, 3, 4, 5 and 6. The slopes of the experimental curves in Figs. 26, 28, 29 and 30 are seen in the case of a single emitter to vary as a function of its emission history. Evidently the work function, which essentially determines the slope, may change as the emitter ages.

Stern, Gossling and Fowler (20, p. 701) report such a dependence of slope upon work function and assign a probable range of  $3 < \phi < 4.5$  for emitters similar to those used here. They report that sodium, or other impurities of low work function, contaminate the emitter surface and furnish considerable emission at low fields. These impurities are "burned off" by the passage of large currents causing the emitter to return to its normal work function. Apparently ordinary out-gassing procedures do not necessarily remove such spots of impurities. The passage of large field currents at high field strength serves to "clean up" the emitting surface.

Müller has observed visually the effects of contamination of the emitting surface by small areas of impurities of low work function. He

notes that scattered impurities on the emitting crystal face tend to accumulate in certain areas as small as  $10^{-11}$  cm<sup>2</sup>. These small areas of low work function contributed most of the emitted current.

Henderson and Dahlstrom (12, p. 475) observed that field emitters tend to emit large unstable currents at first, then settle down to lower current and more stable emission.

These effects have all been verified experimentally, using the several tubes described herein, and are consistent with the assumption that small areas of the emitter are initially contaminated with impurities.

Thus Figs. 28 and 29 may be interpreted as follows. The direct current portion of the curves have slopes differing from those of the pulsed portions in a direction indicating that the direct current data were largely contributed by small areas of impurities of low work function. These emitters were conditioned by continued passage of d-c currents, in an attempt to remove such impurities, and therefore the d-c curves represent stable d-c states at low current densities. In view of the possibility of damage to the point it was not considered wise to pass larger d-c currents than those used. The pulsed portions of the curves have slopes which are steeper than those for d-c operation and are assumed to correspond to work functions of  $\phi = 4.5$  volts for tungsten. This value cannot be far wrong. At worst the work function might conceivably be reduced to 4 volts if tantalum from the anode were deposited in sufficient quantity upon the emitter. Fortunately, the values of J, A, and F derived by this

method are rather insensitive to small changes in  $\phi$ , as will be shown later. A value of  $\phi = 4.5$  volts is therefore assumed to be satisfactory for the pulsed portions of each emitter.

The slopes of the theoretical curves, #7 and #8, may be taken from the dotted straight lines that are plotted in Fig. 31 in order to extend the linear low-field sections of the curves into the region of high fields. This approximation neglects the effect of the small curvature in the theoretical curves at very high fields. The resulting error amounts to less than a factor of 2 in the calculation of  $J$ , and  $A$ , and does not impair the order-of-magnitude-check on theory.

In Fig. 31, curves 1, 2 and 3 correspond to Figs. 28, 29 and 30 in that order. In each case the slope of the pulsed portion of the experimental curves has been drawn parallel to that of the straight line portion of the theoretical curve for  $\phi = 4.5$  volts. This is accomplished by multiplying the  $10^4/V$  values from the experimental curves by the ratio of the slopes of the experimental to the theoretical curves. Values of the  $\log_e i$  remain unchanged.

The experimental curves of Millikan and Eyring (13, p. 55) and of Abbott and Henderson (2, p. 117) are plotted in a similar fashion and appear as curves 5 and 6 respectively, of Fig. 31.

The maximum current densities and the emitting areas shown in Table 2 are measured graphically from Fig. 31. Current densities are taken from the theoretical curve 7, at fields corresponding to the maximum values indicated by the various experimental curves. Areas are calculated upon the assumption that the total current is the

EMITTER IDENTIFICATION	ASSUMED VALUE OF $\phi$	AREA OF EMITTER IN CM <sup>2</sup> (FROM GRAPH)	J, CURRENT DENSITY IN AMPERES PER CM <sup>2</sup> (FROM GRAPH)
# 1 PULSED	4.5	$2 \times 10^{-9}$	$3 \times 10^7$
# 2 PULSED	4.5	$8 \times 10^{-10}$	$3 \times 10^7$
# 2 DIRECT CURRENT		$3 \times 10^{-12}$	$6 \times 10^9$
# 3 PULSED AND D.C.	4.5	$3 \times 10^{-10}$	$1 \times 10^8$
# 3 PULSE AND D.C.	3.0	$1 \times 10^{-10}$	$3 \times 10^8$
MILLIKAN	4.5	$7 \times 10^{-11}$	$9 \times 10^6$
ABBOTT AND HENDERSON	4.5	$1 \times 10^9$	$8 \times 10^3$
EXPERIMENTAL VALUES WITH ELECTRON MICROSCOPE	AREA OF EMITTER IN CM <sup>2</sup>		J, CURRENT DENSITY IN AMPERES PER CM <sup>2</sup>
MÜLLER	$1 \times 10^{-11}$		$1 \times 10^6$

TABLE 2

product of current density and area.

It is convincing that the emitting areas found by this method are in close agreement with those reported by Müller. This argues for the correctness of the method insofar, at least, as orders of magnitude are concerned.

The emitting area from the data of Abbott and Henderson is found to be the largest listed in Table 2 while the maximum current density listed is smallest. As noted in their paper (2, p. 117-118) Abbott and Henderson found the best check between theory and experiment when emitting areas were small and of uniform current density and surface field. Where this is not so, the total current  $i$  becomes a complicated integral of the current density over a larger, non-uniformly emitting area. Abbott and Henderson note that the net effect is a departure from linearity in the  $\log_e i$  versus  $10^4/V$  plots, and observe such a departure experimentally. The calculated values of area and current density made from their data are consistent with the foregoing explanation offered by Abbott and Henderson.

On the other hand, the calculations made from the data of Millikan and Eyring show their emitting areas to be much smaller and their current densities much larger than those of Abbott and Henderson. A more favorable comparison between theory and experiment is to be expected in the former case and it is significant to note that Millikan and Eyring obtained close agreement with theory. Their plots of  $\log_e i/F^2$  versus  $10^4/V$  show no detectable departure from linearity.

Furthermore, the experimental conditions relative to emitter geometry, work function, total current range, etc. are nearly identical to those of Müller, and it is thus significant that the calculated area and current density are in close agreement with the experimental values found by Müller. This has been generally accepted as a conclusive argument for the correctness of the Fowler and Nordheim theoretical equation for current density in all but the highest field regions.

The areas found for the emitters used in this work lie in a small range, centered around the value observed by Müller. The area determined for the direct current portion of the curve for emitter #1 (Curve 1, Fig. 31) is  $3 \times 10^{-12}$  cm<sup>2</sup>, and is listed in Table 2. This is unusually small. Its current density is  $6 \times 10^9$  amperes/cm<sup>2</sup> which is unusually large. Furthermore, from the slope of the d-c portion of curve 1, Fig. 31, the emitter is found to have a work function equal to approximately 3 volts. These observations are consistent with the assumption that this d-c emission comes from a very small spot of surface impurity of low work function.

Figure 32, from Müller's work, shows a photograph of the enlarged emission pattern from a tungsten field emitter. In his Fig. 5c, the small, bright areas are associated with intense emission from impurities. This observed behavior is in close agreement with that predicted from curve 1, Fig. 31. Presumably these small areas are "burned off" at higher fields leaving the larger, more stable emitting area. This may explain the slope of the pulsed portion of curve 2, Fig. 31.

The behavior of the emitter at the high field extremity of the

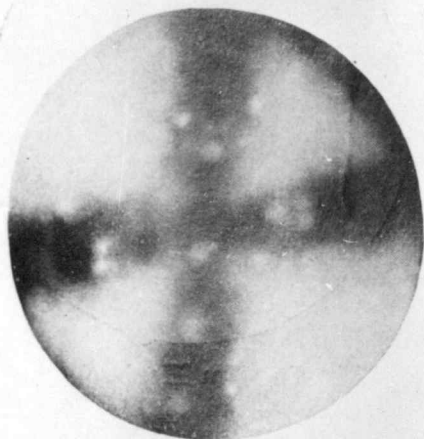


Fig. 5a. Wolframkathode, [011]-  
Richtung in der Mitte, bei 2600° K  
geglüht, 4100 Volt,  $2 \cdot 10^{-5}$  A.

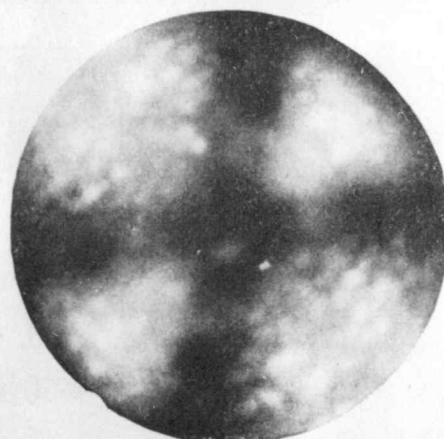


Fig. 5b. 1 min bei 2100° K akti-  
viert, 4000 Volt.

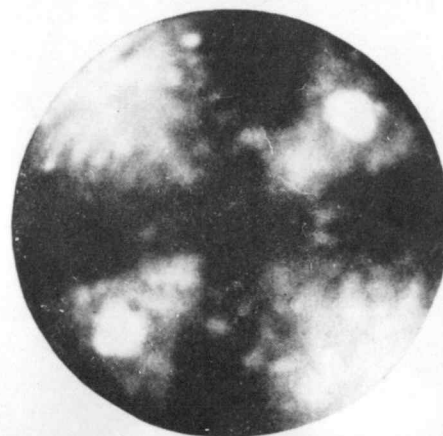


Fig. 5c. 1 min bei 1500° K ge-  
glüht, 3800 Volt, scharf begrenzte  
Thoriumflecke auf den (111)-  
Ebenen.

Fig. 32 Electron microscopic projection of emitting cathode surface showing emission from small spots of impurities of low work function. From Müller (16, p. 545)

pulsed curves is of great interest. No curvature is observed for the pulsed range of Fig. 28 (and curve 1, Fig. 31). These data are considered to be reliable since the currents are well over one hundred times as large as the reliable lower limit of detection of the pulsed current recording apparatus. The reproducibility of these data is remarkably good from pulse to pulse as shown in Fig. 27. From the curve of Fig. 28 it is seen that no curvature in the  $\log_e i$  versus  $10^4/V$  plot exists for the pulsed range of emitter #1. The curvature predicted by theory would be small in the range of current densities covered by pulse measurements; however, it is believed that the predicted curvature, if present, could be detected by the existing apparatus. This slight departure from theory, at these very large current densities, may be in part explained by the effects of space charge. A preliminary study of these effects is reported by Stern, Gossling, and Fowler (20, p. 705-709).

A definite curvature is noted in the pulsed portion of the curve in Fig. 29. The results for emitter #3, Fig. 30, are indecisive in this respect. There exists some doubt as to the validity of the experimental points representing maximum current in the case of each pulse in Figs. 29 and 30. At the leading edge of each current pulse some radiation pick-up from the pulser is possible and may introduce a small error in the recorded peak current value. Experimental points below the current maximum are known to be reliable. It is noted that the curve of Fig. 29 shows a definite curvature in the reliable points, i.e. excluding the highest, and that this

curvature is in a direction supporting the theory. Figure 30 is indecisive in this respect, because a straight line can be drawn through the reliable points for some pulses, as shown in the insert. Figure 28 is strictly linear over the pulsed range where the current varies by a factor of 100. The general conclusion, therefore, is that no curvature in excess of that predicted by theory is observed in the  $\log_e i$  versus  $10^4/V$  graph. It is to be emphasized that all of these results were obtained at large current densities.

It is clear that the emitter will furnish very large currents when its surface barrier is reduced below the value,  $\mu$ , which corresponds to the level of the highest energy electrons in the metal. It would be expected that the behavior of the field emitter would change greatly for small changes of field in the region for which this occurs. An indication as to what may happen to the emitter, under these conditions, is furnished by Rojansky (19, p. 217,219).

The maximum current densities observed from curves 1, 2, and 3, Fig. 31, occur at values of the field remarkably close to the value,  $F = 1.42 \times 10^8$  volts/cm, for which the surface barrier of the metal has been reduced by the amount  $\phi$  to the level  $\mu$ . This value of field is shown by the dashed vertical line in Fig. 31, for  $\phi = 4.5$ . At this value of field the theory of Fowler and Nordheim no longer applies. Those electrons whose energies are above the barrier height have a transmission coefficient which approaches unity as the ratio of electron energy to barrier energy becomes large. Hence these electrons would contribute the major share of the observed field

current in this special case. In view of the large number of free electrons in a metal with energies near the top level  $\mu$ , the field current may be expected to increase enormously as the applied electric field nears and passes the critical value for which the barrier is decreased to  $\mu$ . Some heating of the emitter appears reasonable in view of the large current densities and the small areas and metallic volumes involved. The effect of such heating would be to raise the energies of some of the free electrons in the metals to levels above  $\mu$  in accord with the temperature dependence of the Fermi-Dirac energy distribution. This effect is noted graphically in Fig. 4. Thus when the barrier is lowered to a value slightly above  $\mu$ , (i.e., lowering less than  $\phi$ ), even a relatively small temperature rise would furnish a considerable number of electrons with energies above the barrier. These electrons would contribute significantly to the existing field current. This increase in current in turn would further increase the emitter heating and hence result in an unstable condition. It is reasonable to assume that unstable currents would increase very rapidly with increase in field and would finally result in the formation of a vacuum arc in which the current is carried by electrons and metallic ions. It might be expected, also, that the point of instability would occur at lower values of the electric field in the case of continuous direct current emitters than in the case of pulsed emitters at low recurrence rates. These effects have been observed thus giving further support to the theory of Fowler and Nordheim.

The maximum stable current densities observed in curves 1, 2, and

3, Fig. 31, occur at times near, but below, the upper limit for the theoretical equation for  $\phi = 4.5$ . A further increase of the field by a few percent resulted in instability of the emitter, in the case of curves 1 and 2. These emitters were vaporized following the passage of a brief but brilliant arc. In view of the vacuum, which was better than  $10^{-7}$  mm of Hg, and the thorough preliminary outgassing of the metal parts, it seems likely that the arc consisted of a large current carried by electrons and metallic ions rather than by gaseous ions. The existence of vacuum arcs has been noted by Trump and Van de Graaff (21, p. 327-332), who calculate the probabilities for the liberation of metallic ions by electrons which impinge on metallic anode surfaces. They found that the number of positive metallic ions liberated per incident electron is less than  $1 \times 10^{-3}$  at voltages less than 20 k.v., but increases rapidly at higher potentials. They also found that at corresponding voltages, roughly one electron is liberated per positive ion incident on a metallic surface. The number of electrons also increases rapidly with increasing voltage. Thus in a tube, positive metallic ions liberated at the anode can strike the emitter and liberate more electrons which in turn produce more positive ions. This process becomes cumulative and produces vacuum arcs at potentials around 200 k.v. However, breakdown within the tube at voltages of 20 k.v. or less is attributed by Trump and Van de Graaff to field emission effects. These results are consistent with, and help to explain, the behavior of the field emitter near the point of instability.

The vacuum arc observed in these experiments appears thus to be initiated by large values of the field current. When currents are limited to pulses of a few microseconds duration as in the case in the experiments represented by Figs. 28, 29, and 30, instability and vacuum arcs occur at electric fields near, but slightly below, the critical values predicted by theory. This slight difference between experiment and theory is probably due to resistive heating of the emitter by the high current density, or by positive ion bombardment, of both. Continued vacuum arcs vaporize the emitter. Photographs typical of points which have passed sustained vacuum arcs are shown in Fig. 33. In some cases, the liquified portion of the metal cools in the shape of a spherical cap. In others, a considerable amount of emitter material appears to be transported to the anode surface. In both of these events the geometry of the emitter is greatly changed.

In one case an emitter survived a vacuum arc at very large current levels and returned to its initial state, apparently undamaged. Pulses 1, 2, and 3, Fig. 30, insert, were taken at increasing values of peak voltages. Figures 34, 35, 36, and 37 show the photographs of the voltages and current pulses from which the curves of Fig. 30 were taken. The curves for pulses 2, 3, and 4 correspond to Figs. 34, 35, and 36 respectively. Figure 34 shows the normal behavior of voltage and current curves during a pulse. Figure 35 (pulse 3, Fig. 30) shows the voltage and current pulses during the time of occurrence of a vacuum arc. It is seen that the voltage pulse drops well below its peak value when the arc occurs, as indicated by the

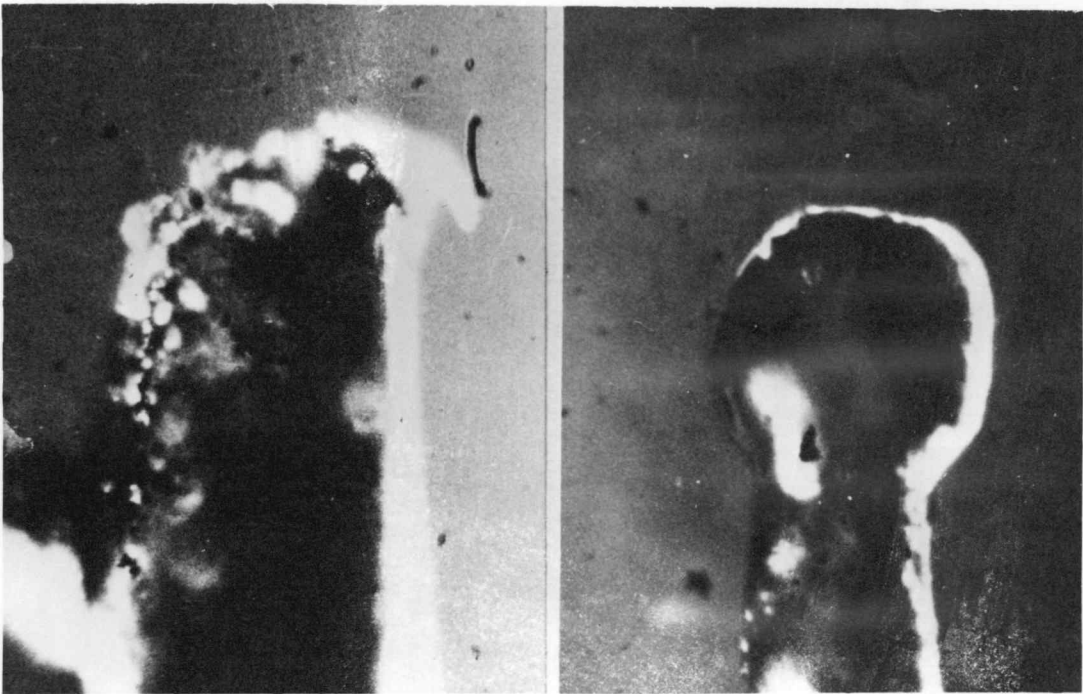
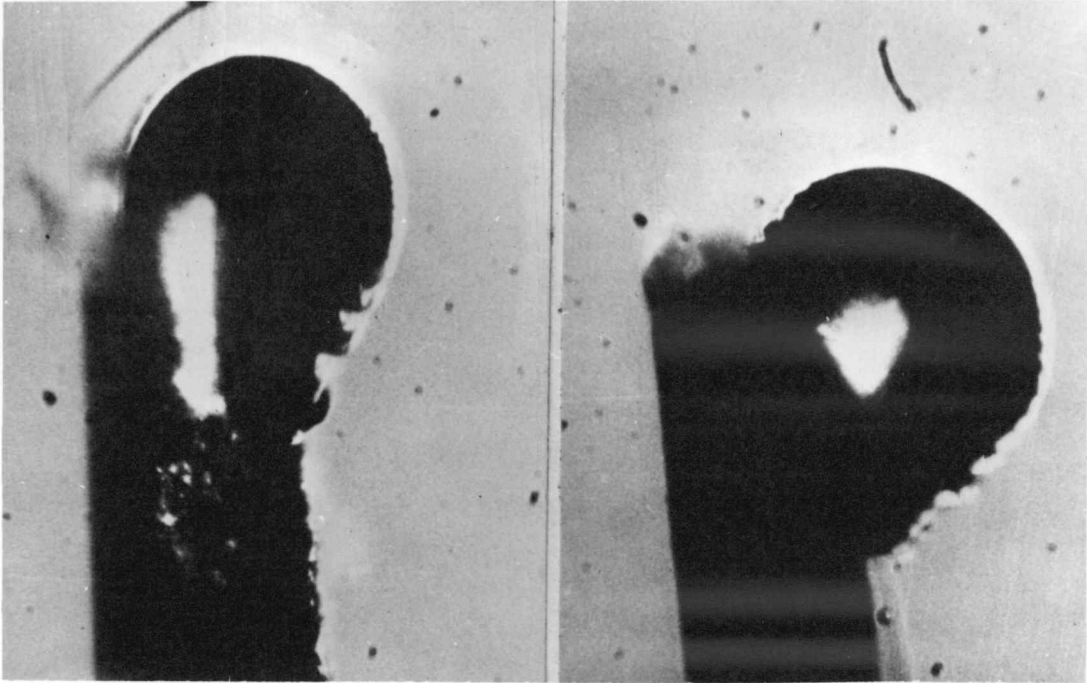


Fig. 33 Typical examples of previously sharp tungsten points after passage of vacuum arc. Magnification 680x.

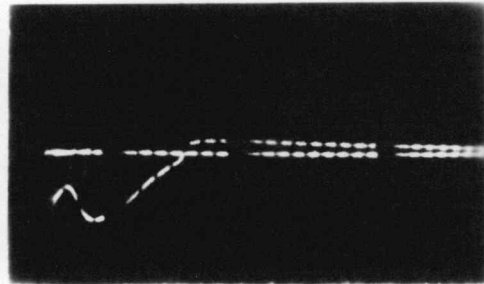
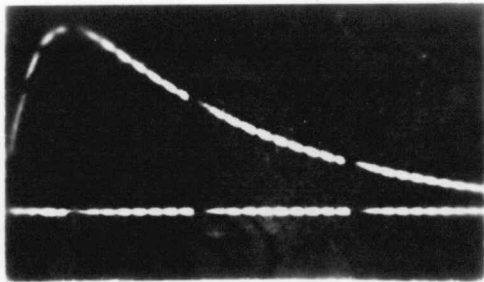


Fig. 34 Normal behavior below region of instability.

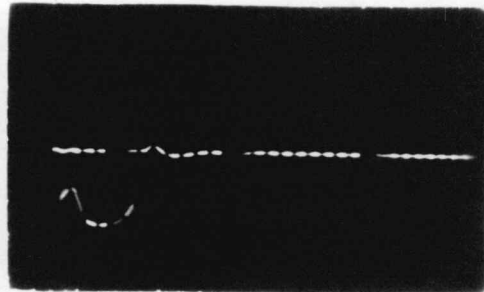
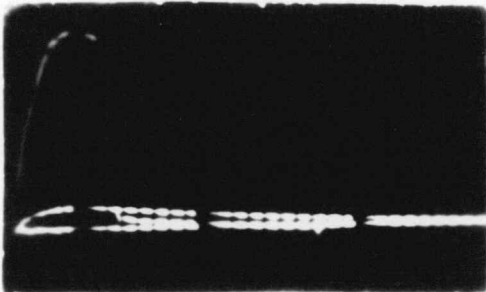


Fig. 35 Behavior during vacuum arc which emitter survived.

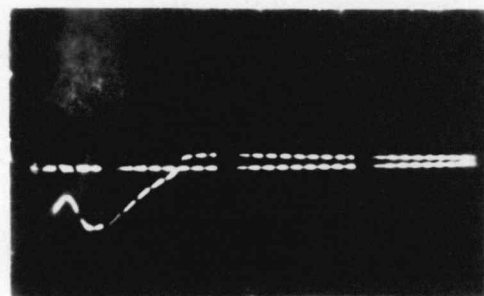
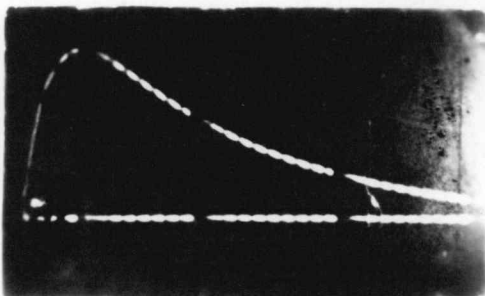


Fig. 36 Normal behavior below region of instability after surviving arc.

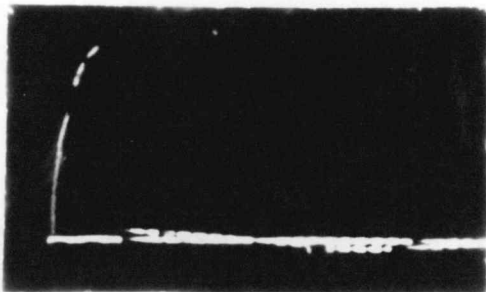


Fig. 37 Behavior during second arc which destroyed emitter. Voltage (left) and current (right) oscilloscope traces for emitter #3.

abrupt termination of the normal oscilloscope trace. Simultaneously the current increases sharply and the current trace is deflected off the oscilloscope face. Figures 34 and 36 (also pulses 2 and 4 of Fig. 30) are for emitter, #3, for pulses applied immediately before and immediately after the vacuum arc which this emitter survived. Figure 35 shows conditions during the vacuum arc. From the similarity between the plots of pulses 2 and 3, Fig. 30, insert, it is apparent that the emitter characteristics remained unchanged in spite of the arc. Figure 37 records the eventual destruction of emitter #3 during a second vacuum arc which occurred some time later. The arc shown in effect in Fig. 35 occurred late in the pulse when much of the energy of the pulse had been dissipated. Presumably this accounts, in part at least, for the survival of this emitter. In Fig. 37, the arc which destroyed the emitter occurred near the voltage peak when maximum energy was available in the pulser.

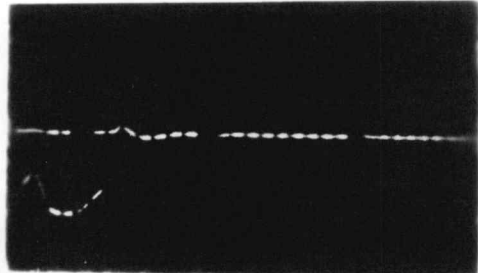
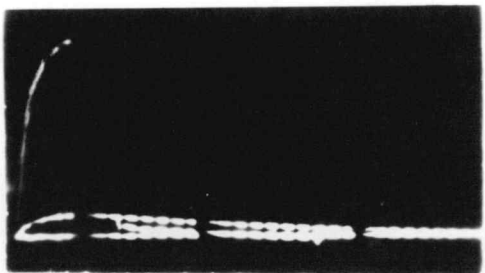
The change recorded by the voltage pulse of Fig. 35, together with elementary circuit analysis leads to an estimate of the current carried by the emitter during the vacuum arc: at least 100 amperes for one microsecond. Thus at the onset of instability the total emitter current changed from a few milliamperes to approximately 100 amperes in much less than a millionth of a second. This is regarded as a remarkable performance, not the least part of which is the fact that the emitter survived.

In Fig. 34 and in pulse 2, Fig. 30, arcing occurred three microseconds after both voltage and current reached their maximum values.

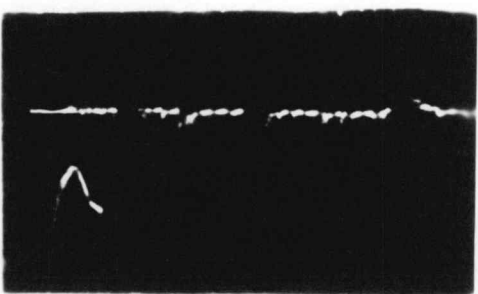
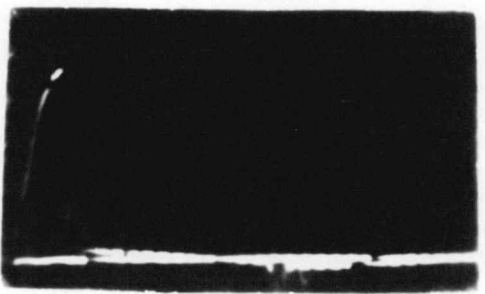
Normally, vacuum arcs occur near the voltage and current peaks. Photographs of four pairs of oscilloscope traces, for voltage and current, taken during vacuum arcs are presented in Fig. 38. The traces of Fig. 34 are included again, at the top, for comparison.

A consideration of the general behavior of arcs of various types suggests that the arc should be expected to occur at or before the voltage and current peaks.

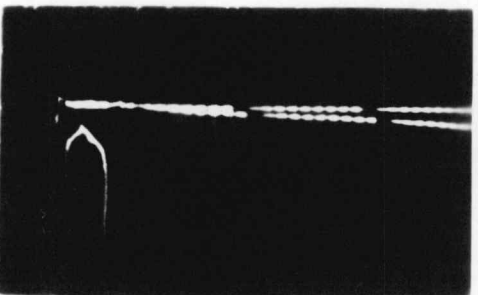
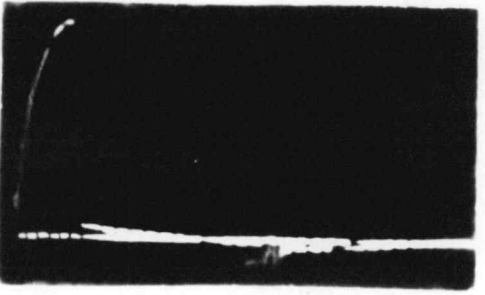
Although in three of the current-voltage pairs of Fig. 38, arcs occur at the voltage peaks, the 3 microsecond delay between voltage maximum and arc formation shown in Fig. 34 suggests that some process within the emitter itself may at times be a controlling factor in determining the time at which an arc starts. For example if considerable heating occurs at the minute emitting areas due to resistive effects, or to positive ion bombardment, it is conceivable that a thermal time lag may exist during which the heat is conducted to other areas of the crystal. As noted above, a small amount of heating could result in emitter instability when, in the presence of very high electric fields, the barrier is reduced to or near the value  $\mu$ . Since it is well known that various crystal faces have work functions differing by a tenth of a volt or so and that this difference is normally enough to cause the greater part of the emission to come from areas which have the slightly lower work functions (Müller 16, p. 544-546) it may then be that a small amount of heating at high fields can result in an increase in the emitting area. This could occur if heating were sufficient to raise electron energies



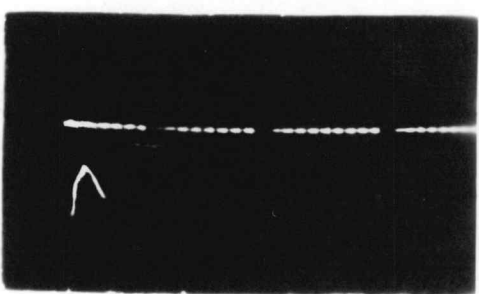
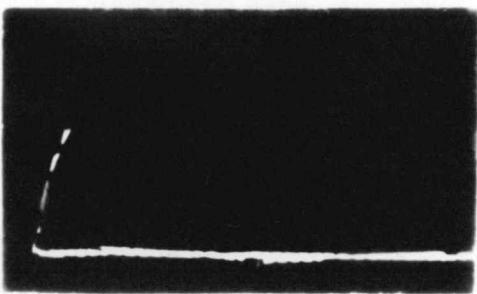
Emitter #3



Emitter #3



Emitter #2



Emitter #1

Fig. 38 Voltage (left) and current (right) oscilloscope traces during four vacuum arcs of three different emitters.

over the barriers of the several crystal faces, if the barrier is lowered to a value approaching  $\mu$  by the presence of the high external field. If such an effect exists it would be expected to be more pronounced near the point of instability.

The series of voltage and current oscillograms shown in Figs. 39, 40 and 41, which were taken during the transition through the point of instability for emitter #2 in Fig. 29, exhibit a peculiar performance which may be attributed to the increase in area due to heating as discussed above. The data for pulses #1 and 2, Fig. 30, were taken from the oscilloscope traces of Figs. 39 and 40, respectively. A comparison of current pulses between Figs. 39 and 40 shows that changes take place in the emitter parameters near the peak of the current curve. In fact it is just at this point, in time, at which the arc occurred in Fig. 41, for the same emitter. The voltage peak in Fig. 39 corresponds to 5600 volts across the point to plane emitter. In Figs. 40 and 41, the peak voltages were 5900 volts.

Evidently the performance shown in Fig. 40 for emitter #2 was obtained for conditions very close to those of instability. Evidence of a change in the characteristics of the emitter is brought out in the insert of Fig. 29, in which data taken from Fig. 40 are plotted as pulse #2 and compared with pulse #1 in Fig. 29 which was plotted from similar data taken from Fig. 39. It is seen that the two curves are displaced vertically although their straight line portions remain sensibly parallel. Thus the values of  $\log_e i$  in pulse 2 are increased by a constant amount over those of pulse 1. This is readily

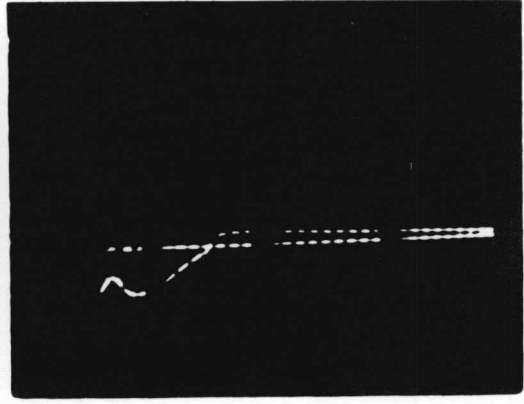
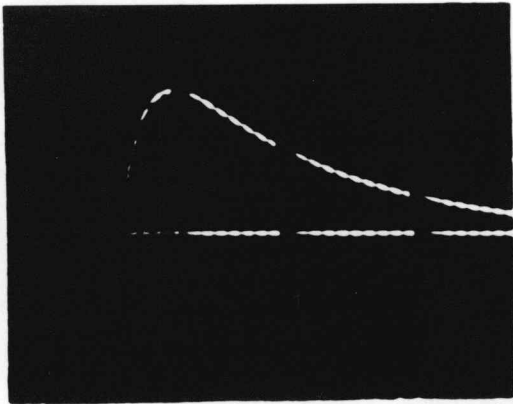


Fig. 39 Normal pulse condition below region of instability.

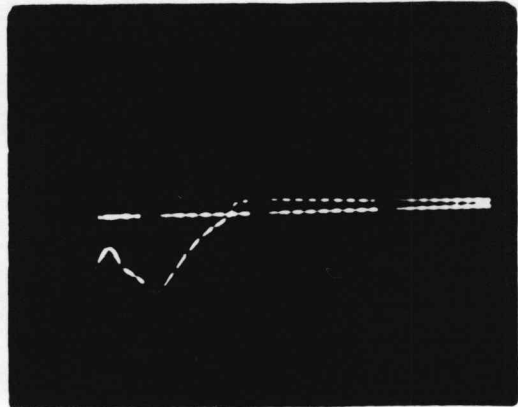
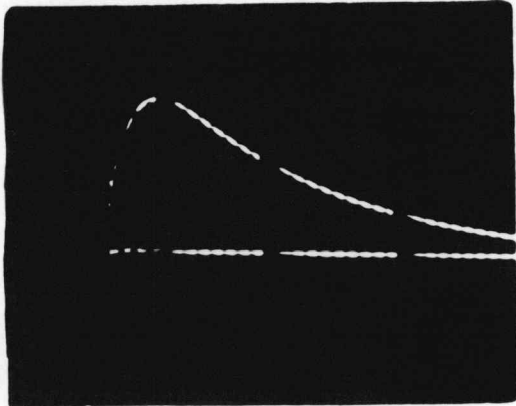


Fig. 40 Abnormal pulse condition bordering region of instability.

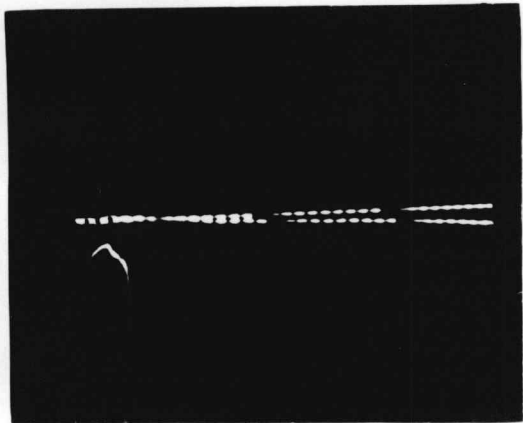
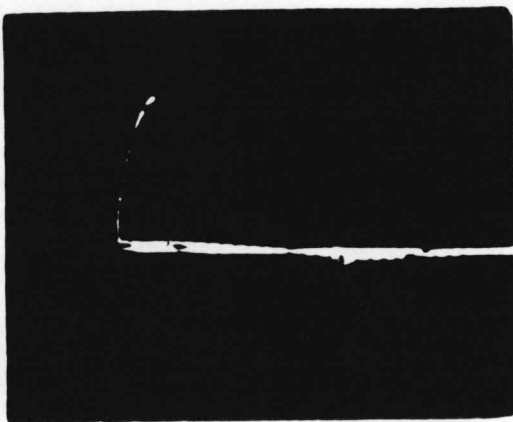


Fig. 41 Pulse condition during vacuum arc.  
Voltage (left) and current (right) oscilloscope traces at  
and near region of instability for emitter #2.

explained by the simple assumption that the area of the emitter is increased between pulse 1 and pulse 2. This area increase may be a result of emitter heating. That the region of instability was approached during pulse 2 is evident from Fig. 31, which indicates that the peak field is approaching a value for which the barrier height is reduced to  $\mu$ . The next pulse at the same applied voltage, shown in Fig. 41, caused a vacuum arc. Thus it was by unusually good fortune that the photographs in Fig. 40 were obtained.

There is considerable additional evidence to indicate that resistive or bombardment heating may influence the process of field emission. Generally speaking these effects are more noticeable for large currents than for small ones, and are greater for direct than for pulsed currents.

Dyke (4, p. 39-44) has observed that a considerable current of electrons having energies greater than  $\mu$  is to be found when the distribution in energy among emitted field electrons is determined experimentally under direct current conditions. Studies at currents up to roughly a microampere from a sharp tungsten point emitter indicate that the effect is negligible at small currents and is appreciable at larger values.

It is well known that direct current emission from sharpened points of small area becomes unstable at total currents in the range from microamperes to milliamperes. Incandescent fragments have been observed to leave the point at higher currents. Eventually the emitter is destroyed, evidently due to heating effects. Further evidence in

support of emitter heating has been observed with the tube shown in Figs. 20 and 21.

This tube is an electron microscope type in which the emitted electrons leave the sharpened tungsten point emitter, pass through a small ring shaped anode and impinge on a fluorescent screen. It is similar in detail to the one used by Müller (16, p. 542.) An anode potential of approximately 6000 volts produced an emission pattern approximately an inch in diameter on the fluorescent screen. Initially the spot appeared on the side of the tube at an angle of approximately  $45^{\circ}$  with the axis of the emitting point. As the anode potential was increased gradually, and as the resulting emitted current reached the value of a few microamperes, the emission pattern increased somewhat in brilliancy, but remained unchanged in position and detail as was to be expected. However after a few minutes of operation at constant potential both the emitted current and visual brilliance of the spot pattern began to increase slowly. At the same time the emission pattern on the screen moved gradually over to the axis of the emitter. It was then necessary to readjust the cameras. The potential across the tube was reduced to zero for a short period during the readjustment. When the potential was subsequently returned to its original value, no emission was observed, nor could any be detected at voltages almost twice as large as those used at the time of the intense emission.

Upon microscopic examination the point appeared as shown in Fig. 43. Initially it was sharp, as in Fig. 42. Apparently, the continued

emission of direct current of the order of microamperes at potentials of approximately 7000 volts had sufficed to melt the point of the emitter. Furthermore, the emitter had evidently continued to emit while in, or near, the molten state. This probably explains the movement of the emitting area across the surface of the emitter, and accounts for the large increase in current and visual brilliance that was observed at constant voltage. Evidently, upon removal of the voltage, the molten emitter was drawn into a sphere by surface forces, and had cooled in this shape. Obviously, the electric field would be greatly reduced in the case of Fig. 43 as compared to Fig. 42. This accounts for the lack of emission when the voltage was re-established.

An electron microscope tube of the type shown in Fig. 22 and 23, employing a linear tungsten filament 0.001 cm in diameter, concentric with a helical anode, was used to observe the emission patterns from linear emitters. The technique is similar to Müller's (16, p. 542) but is adapted to cylindrical symmetry. The emission from the tungsten field emitter passes through the anode and falls on a coating of willemite on the inner surface of the glass walls of the experimental tube, where a magnified image of the emission pattern can be observed, and photographed. Figure 44 reproduces photographs of the enlarged emission pattern from several of the emitters in this tube. Several conclusions may be drawn from these observations.

Apparently only a small fraction of the area of the tungsten wire furnishes emission. This area increases, i.e., more emitting spots appear, as the current and electric field are increased.

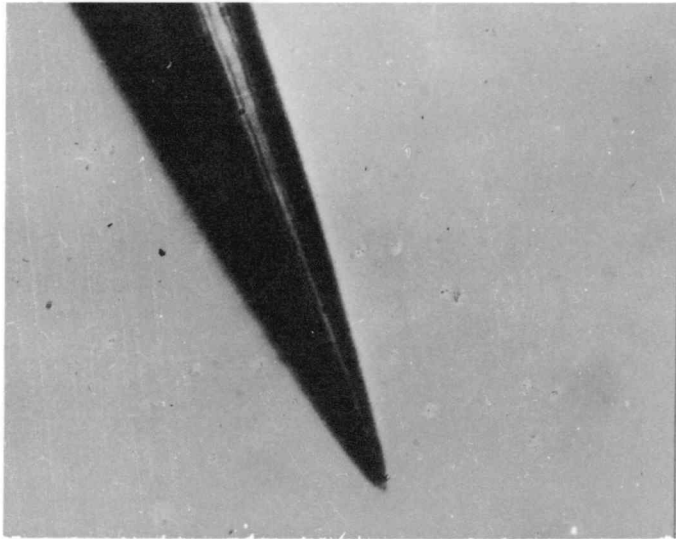


Fig. 42 Emitter point before use. Magnification 2000x.



Fig. 43 Emitter point after use. Magnification 1500x.  
Tungsten emitter used in electron microscope tube, before and after use.

Because the total area of emission is larger for a linear filament than for a sharpened point, much larger direct currents can be drawn from the former before emitter instability sets in. Where a single sharpened point emitter may have as many as four separate well defined areas of emission, a linear wire may have fifty or more such areas.

The main purpose of the investigations using the various electron microscope tubes has been to compare the behavior of the emission patterns for direct current operation with those of pulsed operation. In the few cases that have been studied successfully so far, the emission patterns for direct and stable pulsed currents are identical at similar values of electric field. This is important to the interpretation of the foregoing pulsed data.

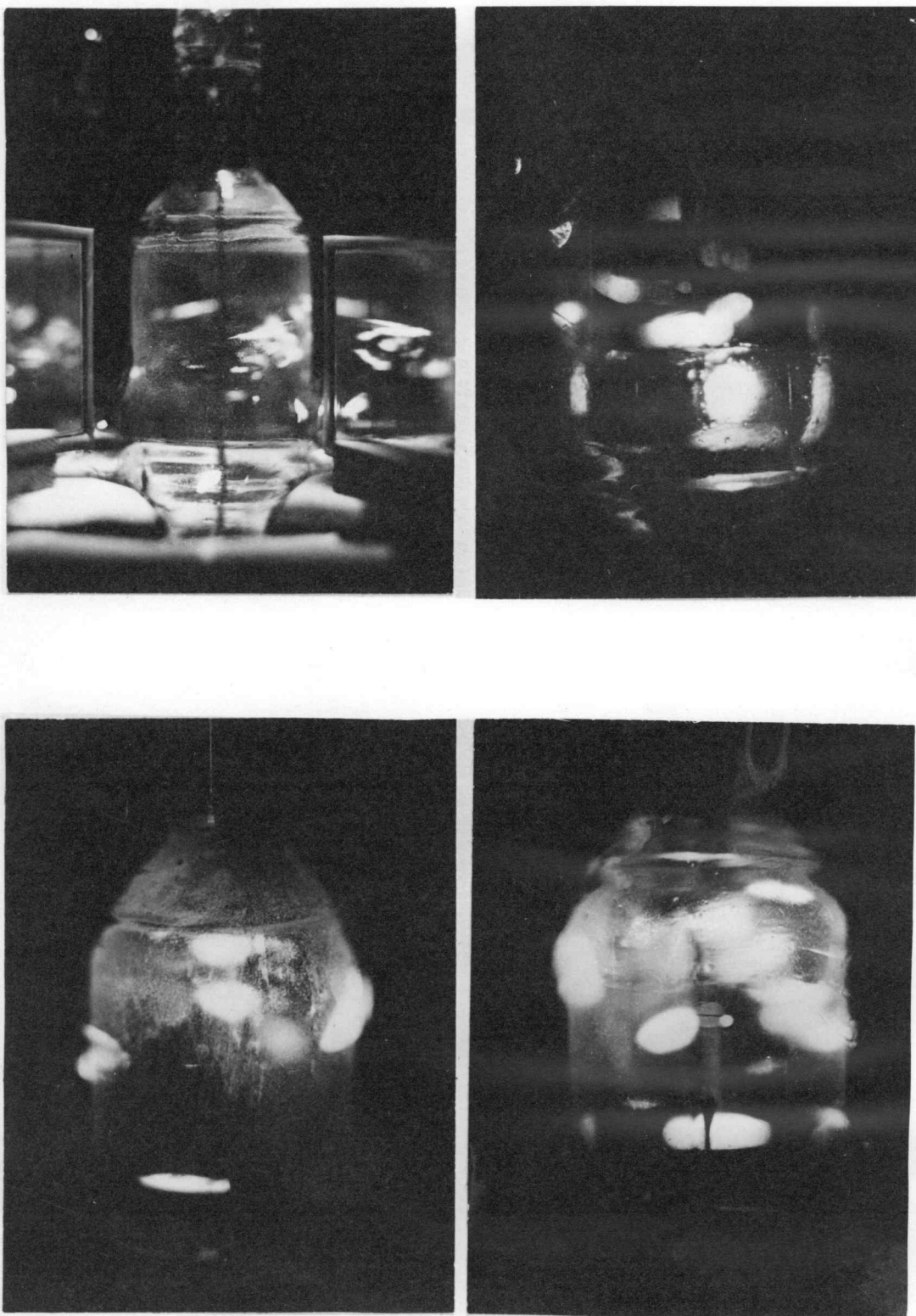


Fig. 44 Emission patterns from electron microscope type field emission tube for different linear tungsten wire emitters.

## SUMMARY

The use of short pulses of voltage has permitted the investigation of high density field emission currents without the emitter damage that occurs with d-c measurements. A plot of  $\log_e i$  versus  $10^4/V$  yields, in most cases, a straight line which confirms the experimental field current law. By assuming a value for the work function of the emitter, the experimental curves can be compared to the theoretical curves in which  $\log_e J$  ( $J$  = current density) is plotted against  $10^8/F$ , where  $F$  is the electric field. This comparison shows order-of-magnitude agreement between theory and experiment. The theoretically predicted deviation at high fields was also observed in the case of one emitter at high current densities. From the graph comparing theory with experiment, current densities and emission areas can be found. The emission areas were found to be between  $10^{-9}$  and  $10^{-12}$   $\text{cm}^2$  and to compare favorably with areas found by other experimenters employing similar type emitters. The maximum current density has been computed to be as high as  $6 \times 10^9$  amperes/ $\text{cm}^2$ . This extends considerably the range over which the law has been verified.

High electric fields approaching values for which the potential barrier is reduced to the level of the most energetic electrons in the metal create vacuum arcs within the tube. The field value for which this occurs corresponds to the upper field limit of the Fowler and Nordheim theory. Beyond this limit new theory must be developed.

A consideration of heating at large current densities upon the

emitter and the effect upon the ensuing vacuum arcs indicates that, at the present pulse lengths, the vacuum arc may occur slightly below the critical field value as computed from theory. In one instance a point emitter passed a current estimated at 100 amperes for a fraction of a microsecond without changing its normal emission characteristics. Further shortening of the pulse lengths may permit repeated pulses at such high current levels and thereby yield pertinent information concerning the nature and cause of the vacuum arc. In future work it is planned to combine the methods used in this research with electron microscope techniques to determine emitter geometry accurately and to provide an experimental means for measuring the electric fields.

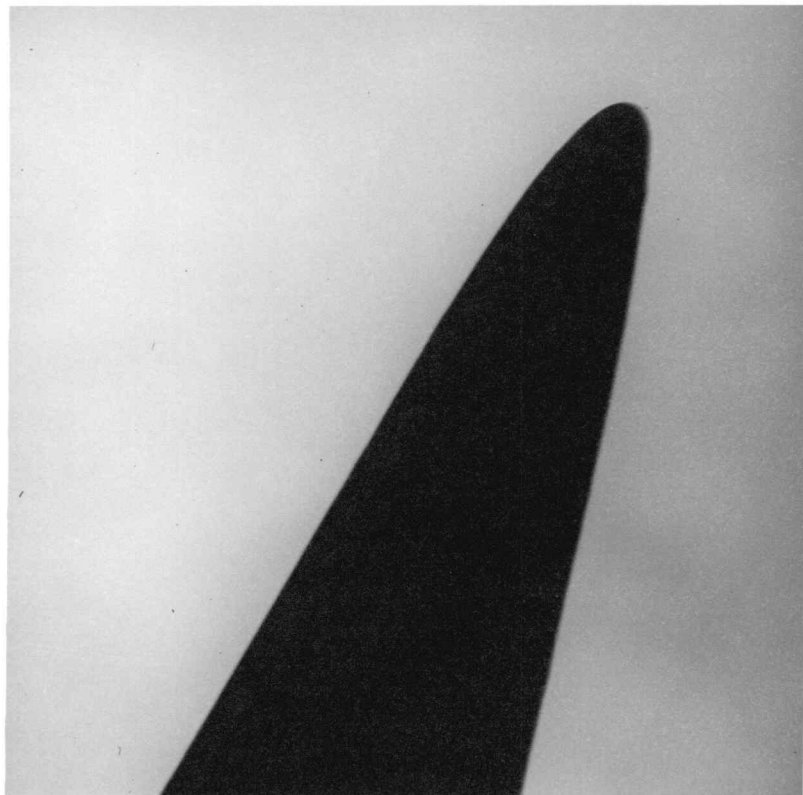


Fig. 45 Electron microscope photomicrograph of a typical, sharp, tungsten point field emitter. Magnification 22,500x.

The electron microscope necessary for resolving sharp points was not available at the time the data for this work were gathered. Thus the value of the electric field could not be computed by geometrical means.

## BIBLIOGRAPHY

1. Abbott, F. R., and Henderson, J. E. The Range and Validity of the Field Current Equation. *Physical Review*, 56:113-118, July 1939.
2. Ahearn, A. J. The Effect of Temperature, Degree of Thoriation and Breakdown on Field Currents from Tungsten and Thoriated Tungsten. *Physical Review*, 50:238-253, August 1936.
3. Dirac, P. A. M. On the Theory of Quantum Mechanics. *Proceedings of the Royal Society*, 112:661-677, October 1926.
4. Dyke, W. P. The Work Functions of Metals from a Field Current Method. Thesis, University of Washington, Seattle: 1-65, 1946.
5. Electrical Engineering Staff of the Massachusetts Institute of Technology, *Applied Electronics*. New York, John Wiley and Sons, Inc., 1943. 772p.
6. Eyring, Carl F., Mackeown, S. S., and Millikan, R. A. Field Currents from Points. *Physical Review*, 31:900-909, May 1928.
7. Fermi, E. Zur Quantelung des Idealen Einatomigen Gases. *Zeitschrift für Physik*, 36:902-912, Mai 1926.
8. Fleming, G. M., and Henderson, J. E. The Energy Losses Attending Field Current and Thermionic Emission of Electrons from Metals. *Physical Review*, 58:887-894, November 1940.
9. Fowler, R. H., and Nordheim, L. Electron Emission in Intense Electric Fields. *Proceedings of the Royal Society*, 119: 173-181, May 1928.
10. General Electric Company of London Staff. The Emission of Electrons under the Influence of Intense Electric Fields. *Philosophical Magazine*, 1 (7): 609-635, March 1926.
11. Henderson, J. E. A Two-Stage Oil Diffusion Pump. *Review of Scientific Instruments*, 6:66-67, March 1935.
12. Henderson, J. E. and Dahlstrom, R. K. The Energy Distribution in Field Emission. *Physical Review*, 55:473-481, March 1939.

13. Millikan, R. A., and Eyring, Carl F. Laws Governing the Pulling of Electrons Out of Metals by Intense Electric Fields. *Physical Review*, 27:52-67, January 1926.
14. Millikan, R. A., and Lauritsen, C. C. Relations of Field Currents to Thermionic Currents. *Proceedings of the National Academy of Science*, 14:45-49, January 1928.
15. Millman, J. and Seeley, S. *Electronics*. New York, McGraw Hill Book Company, 1943. 731p.
16. Müller, E. W. Elektronenmikroskopische Beobachtungen von Feldkathoden. *Zeitschrift für Physik*, 106:541-550, Mai 1937.
17. Nordheim, L. W. The Effect of the Image Force on the Emission and Reflection of Electrons by Metals. *Proceedings of the Royal Society of London, Series A*, 121:626-639, December 1928.
18. Oppenheimer, J. R. Three Notes on the Quantum Theory of Aperiodic Effects. *Physical Review*, 31:66-81, January 1928.
19. Rojansky, V. *Introductory Quantum Mechanics*, New York, Prentice-Hall, Inc., 1938. 544p.
20. Stern, T. E., Gossling, B. S., and Fowler, R. H. Further Studies in the Emission of Electrons from Cold Metals. *Proceedings of the Royal Society of London, (A)* 124: 699-723, July 1929.
21. Trump, I. G., and Van de Graaff, R. J. The Insulation of High Voltages in Vacuum. *Journal of Applied Physics*, 18:327-332, March 1947.